Thermal conductivity and thermal Hall effect in Bi- and Y-based high-T_c superconductors[*]

B. Zeini[1], A. Freimuth[1,a], B. Büchner[1], M. Galffy[1], R. Gross[1,b], A.P. Kampf[2], M. Kläser[3], G. Müller-Vogt[3], and L. Winkler[4]

[1] II. Physikalisches Institut, Universität zu Köln, 50937 Köln, Germany
[2] Theoretische Physik III, Institut für Physik, Universität Augsburg, 86135 Augsburg, Germany
[3] Kristall- und Materiallabor, Universität Karlsruhe, 76128 Karlsruhe, Germany
[4] 2. Physikalisches Institut, RWTH Aachen, 52056 Aachen, Germany

Abstract. Measurements of the thermal conductivity (k_{xx}) and the thermal Hall effect (k_{xy}) in high magnetic fields in Y- and Bi-based high-T_c superconductors are presented. We describe the experimental technique and test measurements on a simple metal (niobium). In the high-T_c superconductors k_{xx} and k_{xy} increase below T_c and show a maximum in their temperature dependence. k_{xx} has contributions from phonons and quasiparticle (QP) excitations, whereas k_{xy} is purely electronic. The strong increase of k_{xy} below T_c gives direct evidence for a strong enhancement of the QP contribution to the heat current and thus for a strong increase of the QP mean free path. Using k_{xy} and the magnetic field dependence of k_{xx} we separate the electronic thermal conductivity (k_{xx}^{el}) of the CuO$_2$-planes from the phononic thermal conductivity (k_{xx}^{ph}). In YBa$_2$Cu$_3$O$_{7-\delta}$ k_{xx}^{el} shows a pronounced maximum in the superconducting state. This maximum is much weaker in Bi$_2$Sr$_2$CaCu$_2$O$_{8+\delta}$, due to stronger impurity scattering. The maximum of k_{xx}^{el} is strongly suppressed by a magnetic field, which we attribute to the scattering of QPs on vortices. An additional magnetic field independent contribution to the maximum of k_{xx} occurs in YBa$_2$Cu$_3$O$_{7-\delta}$, reminiscent of the contribution of the CuO-chains, as determined from the anisotropy in untwined single crystals. Our data analysis reveals that below T_c as in the normal state a transport (τ) and a Hall (τ_H) relaxation time must be distinguished: The inelastic (*i.e.* temperature dependent) contribution to τ is strongly enhanced in the superconducting state, whereas τ_H displays the same temperature dependence as above T_c. We determine also the electronic thermal conductivity in the normal state from k_{xy} and the electrical Hall angle. It shows an unusual linear increase with temperature.

PACS. 74.72.-h High T_c compounds – 74.25.Fy Transport properties (electric and thermal conductivity, thermoelectric effects, etc.)

1 Introduction

Heat transport in the superconducting state is well known to provide valuable information on the quasiparticle (QP) excitations and their dynamics. For example, the order parameter symmetry as well as the QP relaxation time can be obtained by analyzing the thermal conductivity, k_{xx}. Compared to other probes of the QP-dynamics, such as the microwave conductivity, thermal transport has the advantage of probing *only* the QP-response, since the superfluid does not carry heat.

A characteristic feature of YBa$_2$Cu$_3$O$_{7-\delta}$ close to optimum doping is a pronounced maximum of the thermal conductivity in the superconducting state [1–14]. The position and the height of this maximum depend strongly on the sample quality and it is suppressed by a magnetic field [3–5,10,14]. The interpretation of this behavior in terms of QP-dynamics requires a drastic suppression of the QP-scattering rate below T_c, which overcompensates the decrease of the number of QPs [7]. Such a behavior of the scattering rate has been inferred earlier from the microwave surface resistance [15–19]. It provides strong evidence for an electronic origin of the scattering processes in the cuprates. Yet, the interpretation of the maximum of k_{xx} is ambiguous, since in the cuprates a substantial part of the heat is carried by phonons. The phononic contribution k_{xx}^{ph} to the thermal conductivity may also be enhanced below T_c, since the scattering of phonons on electrons is reduced in the superconducting

state [1,6,8]. Such a behavior of k_{xx}^{ph} is known from conventional superconductors [1].

A separation of the QP- and phonon heat currents is difficult. Usually it is attempted on the basis of the Wiedemann-Franz law, which relates k_{xx}^{el} to the electrical conductivity σ_{xx}, i.e. $k_{xx}^{el} = LT\sigma_{xx}$, where L is the Lorenz-number. However, in the superconducting state this requires a (model dependent) determination of the QP-contribution to σ_{xx} from the combined superfluid and QP-response to electric fields [15]. Moreover, in contrast to the normal state, in a superconductor L may be temperature dependent even for purely elastic scattering, as a consequence of different coherence factors for electrical and thermal transport effects [20]. Another approach towards a separation of k_{xx}^{el} and k_{xx}^{ph} is to exploit the magnetic field dependence of k_{xx} [10]. However, since both the electronic and the phononic heat current may in principle depend on the magnetic field [10,21,22], additional information on one of the contributions must be inferred from other experimental data. Finally, it has been attempted to determine k_{xx}^{ph} from measurements of the thermal conductivity of the insulating parent compounds of the cuprates [12]. This is, however, also ambiguous, since the thermal conductivity of these insulators is doping dependent and shows anomalous behavior itself, possibly due to magnetic contributions to the heat current [12] or due to stripe phases [23] and tilt distortions [24] and their coupling to the phonons.

It is therefore useful to measure the transverse thermal conductivity k_{xy}, also called the Righi-Leduc or thermal Hall effect, in addition to the field dependent thermal conductivity [25–30]. The Righi-Leduc effect is the thermal analogon of the Hall effect. It has been pointed out in references [25,26] that phonons do not contribute to k_{xy}, i.e. k_{xy} is purely electronic and contains direct information on the QP relaxation time. However, regarding transport in a magnetic field one additional complication arises: Detailed studies of the normal state electrical transport phenomena show that a consistent description of the experimental data requires the distinction of two relaxation times in the cuprates [33,34]. A longitudinal (transport) relaxation time τ enters the dc conductivity $\sigma_{xx} \propto \tau$, whereas a transverse Hall relaxation time τ_H enters the Hall conductivity $\sigma_{xy} \propto \tau\tau_H$ and thus determines the Hall angle $\tan\alpha_H = \sigma_{xy}/\sigma_{xx} \propto \tau_H$. Experimentally, from σ_{xx} and σ_{xy}, τ and τ_H have distinctly different temperature dependencies. Given this behavior of electrical transport properties one expects a similar scenario also for the (electronic) thermal transport, i.e. $k_{xx} \propto \tau$ and $k_{xy} \propto \tau\tau_H$.

There are further complications in the interpretation of experimental results. In YBa$_2$Cu$_3$O$_{7-\delta}$ CuO-chains are present along the b-direction of the orthorhombic crystal structure in addition to the CuO$_2$-planes common to all HTSCs. These chains lead to a rather strong in-plane (a-b) anisotropy of the electronic properties [31–33] and in particular of the electronic thermal conductivity [7,11]. Moreover, in the superconducting state vortices carry heat and they are known to move in an applied temperature gradient [35,36]. They contribute therefore to the longitu-

dinal and transverse heat currents, if their motion is not prevented by pinning [37]. In the cuprates this contribution may be present in a wide range of temperatures and magnetic fields above the irreversibility line.

In this paper we present measurements of the thermal conductivity and the thermal Hall effect of YBa$_2$Cu$_3$O$_{7-\delta}$ (YBCO) and Bi$_2$Sr$_2$CaCu$_2$O$_{8-\delta}$ (BSCCO) in high magnetic fields. k_{xx} and k_{xy} are found to increase below T_c and to show a maximum in their temperature dependence in both, Bi- and Y-based materials. Since k_{xy} is purely electronic this tells that the quasiparticle heat current is strongly enhanced below T_c, which gives direct evidence for a strong increase of the QP mean freepath. We separate the QP from the phononic contribution using k_{xy} and the magnetic field dependence of k_{xx}. The main results from this data analysis are: (1) $k_{xx}^{el}(B)$ shows a pronounced maximum below T_c which is strongly suppressed by a magnetic field. (2) An additional magnetic field independent maximum of the thermal conductivity is found in YBCO, reminiscent of the contribution to k_{xx} due to the CuO-chains. (3) For k_{xx}^{ph} we find no indication of a maximum or of a significant magnetic field dependence. (4) The vortex contribution to k_{xy} is negligibly small compared to the QP- and phononic contributions. (5) Our data analysis reveals distinct Hall and transport relaxation times, consistent with what is known for the normal state of the cuprates [33,34]. The transport relaxation time is strongly enhanced below T_c and becomes magnetic field dependent, whereas the Hall relaxation time shows the same field and temperature dependence in the superconducting and in the normal state. (6) We determine the electronic thermal conductivity in the normal state from k_{xy} and the electrical Hall angle. $k_{xy}^{el}(T > T_c)$ exhibits an unusual linear temperature dependence.

2 Theoretical background

2.1 Thermal transport

2.1.1 Definitions

Thermal transport is usually described [38] in analogy to electrical transport, i.e. one defines a thermal conductivity tensor $\underline{k}^{el}$ via

$$\mathbf{j}_h = -\underline{k}\nabla T \qquad (1)$$

in analogy to the electric conductivity tensor $\underline{\sigma}$ defined by $\mathbf{j} = \underline{\sigma}\mathbf{E}$. Here $\mathbf{j}$ and $\mathbf{j}_h$ are the electric and heat current density, respectively, $\mathbf{E}$ is the electric field and T is the temperature.

For our discussion of the cuprates we choose the x-, y-, and z-directions along the orthorhombic a, b, and c-directions, where the c-direction is perpendicular to the CuO$_2$-planes. When a magnetic field is applied along the z-direction the transport tensors have 4 independent

coefficients each, *i.e.*

$$\underline{k} = \begin{pmatrix} k_{xx} & k_{xy} & 0 \\ -k_{xy} & k_{yy} & 0 \\ 0 & 0 & k_{zz} \end{pmatrix} \qquad (2)$$

and similarly for the conductivity tensor. If twined crystals are studied the number of components is reduced further, since $k_{xx} = k_{yy}$ and $\sigma_{xx} = \sigma_{yy}$. Experimentally the components of the electrical ($\underline{\rho}$) and thermal resistivity ($\underline{W}$) tensors are measured. The components of $\underline{\sigma}$ and $\underline{k}$ are obtained by inversion of $\underline{\rho}$ and $\underline{W}$, which yields *e.g.* for the in-plane components of $\underline{k}$: $k_{xx} = W_{yy}/D$; $k_{yy} = W_{xx}/D$ and $k_{xy} = -W_{xy}/D$ where $D = W_{xx}W_{yy} + W_{xy}^2$.

Consider a situation where a magnetic field is applied along the z-direction and an electrical current flows along the x-direction, *i.e.* $\mathbf{j} = (j_x, 0, 0)$. Then, due to the Hall effect, an electrical field E_y develops in the y-direction. In complete analogy a thermal Hall effect occurs if we substitute $\mathbf{j} \rightarrow \mathbf{j}_\mathrm{h}$ and $\mathbf{E} \rightarrow -\nabla T$. In this case a heat current $j_{\mathrm{h},x} = -k_{xx}\nabla_x T$ along the x-direction leads to a transverse temperature gradient $\nabla_y T$ in the y-direction, if no heat current in the y-direction is allowed to flow, *i.e.* if $j_{\mathrm{h},y} = 0$. This is the Righi-Leduc or thermal Hall effect. Applying equations (1) and (2) to this situation yields

$$j_{\mathrm{h},y} = 0 = k_{xy}\nabla_x T - k_{yy}\nabla_y T \qquad (3)$$

and thus

$$k_{xy} = k_{yy}\frac{\nabla_y T}{\nabla_x T} . \qquad (4)$$

In the following we distinguish an electrical (α_H) and a thermal (α_R) Hall angle by defining:

$$\tan \alpha_\mathrm{H} = \frac{\sigma_{xy}}{\sigma_{yy}} = \frac{E_y}{E_x} \qquad (5)$$

and

$$\tan \alpha_\mathrm{R} = \frac{k_{xy}}{k_{yy}} = \frac{\nabla_y T}{\nabla_x T} . \qquad (6)$$

For completeness, we mention that a Righi-Leduc coefficient $R_\mathrm{R} = \nabla_y T / j_{\mathrm{h},x} B_z$ is defined in analogy to the Hall coefficient $R_\mathrm{H} = E_y / j_x B_z$.

2.1.2 Phonon contribution to the heat current

In the preceding section we have considered the electronic thermal and electrical transport processes. Naturally there is also a phonon contribution to the heat flow. In simple metals this contribution is usually much smaller than that of the conduction electrons and may be neglected. However, this is not always the case and certainly not for the cuprates, where a substantial part of the heat current is phononic [1]. In this case, defining the phononic and electronic thermal conductivity tensors $\underline{k}^\mathrm{ph}$ and $\underline{k}^\mathrm{el}$,

respectively, the total thermal conductivity tensor of equation (1) is given by

$$\underline{k} = \underline{k}^\mathrm{el} + \underline{k}^\mathrm{ph}. \qquad (7)$$

Note that if other channels of heat conduction are present the corresponding tensors must be added.

It has been pointed out in references [25, 26] that $\underline{k}^\mathrm{ph}$ is usually diagonal even for $\mathbf{B} \neq 0$. In this case the total transverse thermal conductivity k_{xy} is electronic. We shall make this assumption throughout this paper and set $k_{xy}^\mathrm{el} \equiv k_{xy}$ in the following. With the experimental conditions appropriate for the measurement of the Righi-Leduc effect (as defined in the previous section) we find from equations (4) and (7):

$$k_{xy} \equiv k_{xy}^\mathrm{el} = k_{yy}\frac{\nabla_y T}{\nabla_x T} = k_{yy}^\mathrm{el} + k_{yy}^\mathrm{ph} \ \frac{\nabla_y T}{\nabla_x T} . \qquad (8)$$

Clearly, k_{xy} can be determined experimentally by measuring $\nabla_y T$, $\nabla_x T$ and the *total* thermal conductivity k_{yy}. Note that, whereas k_{xy} is purely electronic, the thermal Hall angle $\tan \alpha_\mathrm{R}$ (Eq. (6)) as obtained from the measured temperature gradients is in general *not*.

2.1.3 Wiedemann-Franz law

According to standard transport theory the *electronic* thermal and electrical conductivities are related by the Wiedemann-Franz law. This law in its general form relates the corresponding tensors:

$$\underline{k}^\mathrm{el} = LT\underline{\sigma}. \qquad (9)$$

Here L is the Lorenz number, which for free electrons has the value $L_0 = (\pi^2/3)(k_\mathrm{B}/e)^2 \simeq 2.44 \times 10^{-8}$ (V/K)^2. The Wiedemann-Franz law is valid under rather general conditions and does in particular not rely on the relaxation time approximation. In the normal state it holds if (i) scattering processes are elastic and (ii) if any energy dependence of the collision integral may be neglected. In the superconducting state the situation is more complicated: Even for purely elastic scattering the Wiedemann-Franz law may not be fulfilled, because of different coherence factors for electrical and thermal transport [20].

Taking the magnetic field along the z-direction, the free electron result for $\underline{\sigma}$ and $\underline{k}^\mathrm{el}$ is

$$\underline{k}^\mathrm{el} = L_0 T\underline{\sigma} = L_0 T\sigma_0 \begin{pmatrix} \frac{1}{1+\alpha^2} & -\frac{\alpha}{1+\alpha^2} & 0 \\ \frac{\alpha}{1+\alpha^2} & \frac{1}{1+\alpha^2} & 0 \\ 0 & 0 & 1 \end{pmatrix}. \qquad (10)$$

Here $\sigma_0 = ne^2\tau/m$ is the Drude-conductivity, n is the electron density, and m the effective mass. $\alpha = \omega_\mathrm{c}\tau$, where $\omega_\mathrm{c} = eB/m$ is the cyclotron frequency. The Hall angles are then given by

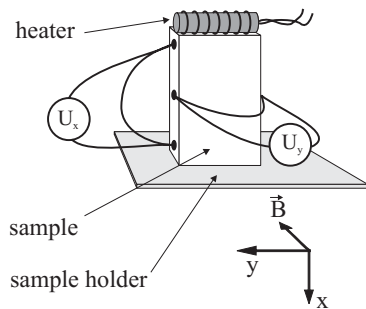$$\tan \alpha_\mathrm{R} = \tan \alpha_\mathrm{H} = \omega_\mathrm{c}\tau. \qquad (11)$$

Fig. 1. Schematic setup used for the measurements (see text).

2.2 Hall and transport relaxation times

In simple metals it is usually sufficient to describe the longitudinal and transverse transport properties using a single relaxation time τ. In contrast, it is well known that in the cuprates a consistent description of the data on such a basis is not possible [33,34]. The reason is that $\tan\alpha_H$ as measured from the Hall effect and the resistivity has a temperature dependence *different* from that of σ_{xx} (see also Fig. 5). In optimally doped samples it is found that

$$\sigma_{xx} \propto \tau \propto T^{-1}, \tag{12}$$

whereas

$$\tan\alpha_H = \omega_c \tau_H \propto T^{-2}. \tag{13}$$

Since the effective (cyclotron) mass entering $\omega_c = eB/m$ is usually temperature independent [39] it is common to define a Hall relaxation time τ_H to account for the temperature dependence of $\tan\alpha_H$ (see *e.g.* [33,34]).

Several scenarios have been proposed in order to justify the use of two relaxation times for the normal state transport properties of the cuprates, reaching from a breakdown of Fermi-liquid theory in favor of a novel metallic groundstate to more conventional scenarios, which exploit a strongly anisotropic scattering rate over the Fermi surface [40–49]. We shall discuss these issues in more detail below. At this point we regard the distinction between τ and τ_H as a definition, introduced to obtain a consistent description of the experimental data. Nevertheless, given the distinction of τ and τ_H from electrical transport one expects on the basis of the Wiedemann-Franz-law a similar distinction for the electronic thermal transport properties, *i.e.* $k_{xx}^{\text{el}} \propto \tau$ and $k_{xy} \propto \tau\tau_H$.

3 Experimental

3.1 Measurements

All measurements were performed with the magnetic field parallel to the c-direction and all temperature gradients, currents, and voltages perpendicular to the c-direction.

For the measurements of $\underline{k}$ a longitudinal temperature gradient was produced by a manganin heater mounted on
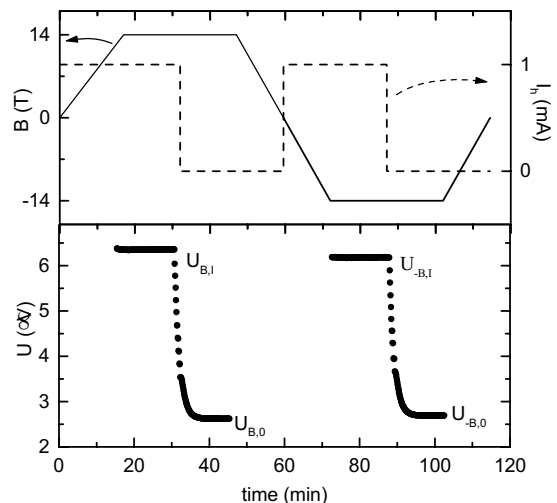

Fig. 2. Upper panel: Variation of the magnetic field B (full line) and the heating current I_h (dotted line) as a function of time. Lower panel: Time dependence of the thermovoltage $U_y \propto \nabla_y T$. The voltages within the plateaus are constant within ± 5 nV.

top of the sample (Fig. 1). The temperature gradients were measured with AuFe-Chromel thermocouples which were calibrated carefully in magnetic fields up to 14 T (see below). All measurements were carried out under adiabatic conditions (*i.e.* $j_{h,y} = 0$) at constant temperature and magnetic field. We used a *Lakeshore 93CA* temperature controller and *Cernox CX-1050* sensors to measure and to control the temperature of the sample holder. The temperature stability achieved in our measurements was better than ± 5 mK. Typically, temperature gradients $\nabla_x T$ of the order of 0.5 K/mm were applied. The resulting transverse temperature gradients $\nabla_y T$ in magnetic fields of order 10 T were of order 0.01 K/mm. The resolution of the thermocouple voltage is of the order ± 5 nV. It is determined basically by the stability of the sample temperature and it allows for the determination of temperature gradients with a resolution in the range of mK.

Since $\nabla_y T/\nabla_x T \ll 1$ in the weak field limit exploited in our experiments one has to separate offset voltages due to misalignment of the thermocouple in the determination of the transverse temperature gradient $\nabla_y T$. We have therefore measured for both orientations $\pm \mathbf{B}$ of the magnetic field in order to determine the component of $\nabla_y T$ which is asymmetric with respect to reversal of the field direction. Figure 2 shows a typical measurement run at a fixed temperature. After the heater is turned on a steady state is achieved within 5 to 15 min. Then the heater is turned off in order to determine the background thermopower. The same procedure is repeated after reversal of the magnetic field. $\nabla_y T$ can then be determined from

$$U_y = \frac{(U_{B,I} - U_{B,0}) - (U_{-B,I} - U_{-B,0})}{2} . \tag{14}$$

where I and 0 correspond to finite and zero heater current, respectively. The magnetic field was reversed at fixed temperature for temperatures above the irreversibility
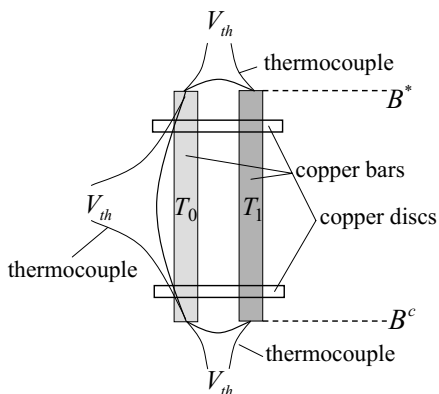
Fig. 3. Experimental setup used for the calibration of the thermocouple for the temperature range between 4.2 and 30 K (see text).
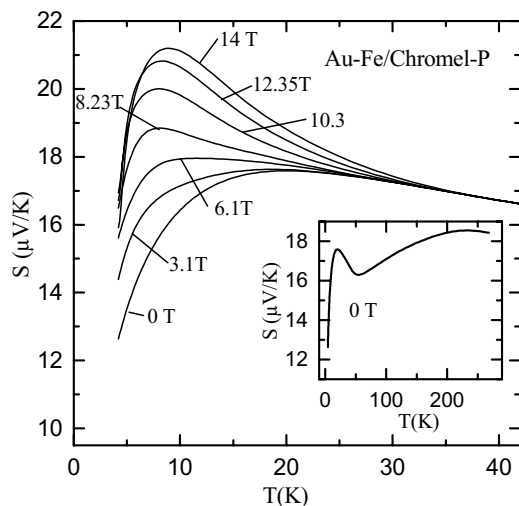

Fig. 4. Thermopower of the thermocouple *versus* temperature at various fixed magnetic fields given in the figure. The inset shows the zero field thermopower in a larger temperature range. Above about 40 K S is only weakly field dependent ($\Delta S/S \leq 4\%$).

line [35]. For measurements below the irreversibility line we have heated the sample to temperatures above T_c before the field was reversed in order to avoid errors due to pinning effects. The Cernox sensors used here have a weak magnetic field dependence ($\Delta T/T$ is less than 0.7% for 14 T). However, this field dependence does not lead to errors in our measurements because it is symmetric with respect to field reversal.

We have also measured the in-plane resistivity ρ and the Hall coefficient R_H using a standard ac-lock-in technique.

3.2 Calibration

For our experiments we have used Au/0.07 at.% Fe Chromel P type thermocouples (Leico Industries Inc.). These thermocouples have a rather small diameter of 0.076 mm to avoid a thermal short circuit when mounted

to the sample, and furthermore they have a good sensitivity in the temperature range from 4.2 K to room temperature. However, because of their magnetic field dependent thermopower $S(B)$ a calibration for measurements in high magnetic fields is necessary. We have calibrated the magnetic field dependence accurately by using two different methods: For the temperature range above 30 K the calibration was done using a piece of α-quartz crystal. With the same setup as for the measurements of the thermal conductivity, the thermocouple and a small heater were mounted on the quartz crystal. As the thermal conductivity of quartz does not depend on the magnetic field, $S(B)/S(B=0)$ can be determined directly for different temperatures by sweeping the magnetic field (for a constant heater power). We have found that above about 40 K the magnetic field dependence of the thermopower is weak ($\Delta S/S \leq 4\%$).

Below 30 K the calibration according to the method described above turned out to be problematic: The small field dependence of the Cernox sensors causes temperature variation of the sample holder as the magnetic field is swept. This leads to errors, because the temperature dependence of the thermal conductivity of quartz is large in this temperature range. We have therefore used a different method for the calibration between 4.2 K and 30 K. Figure 3 shows the experimental setup. We used two copper bars ($l = 130$ mm), one of them with an attached heater wire which was wound regularly around it. The two bars were in thermal contact *via* two copper discs and ^{4}He gas. A well defined temperature difference could be maintained between the copper bars. Three thermocouples were mounted to this setup as shown in Figure 3. The thermocouple mounted along one of the bars was used to check that no temperature gradient builds up along the bars during the measurements. The setup was placed in the magnet with one end in its center ($B = B^c$) and the other end being in a much smaller magnetic field ($B^* = 0.331B^c$). The magnetic field was swept continuously from zero to 14 T measuring $S(B^c)/S(B^*)$ at various fixed temperatures. Using these data $(S(B)/S(B=0))_{T=\mathrm{const.}}$ was determined. Figure 4 shows the thermopower $S(T)$ of the thermocouple as determined for different magnetic fields from $(S(B)/S(B=0))_{T=\mathrm{const.}}$ and the zero field $S(T)$ calibration. Note that the accuracy of our measurements of the field dependent thermal conductivity is determined mainly by the magnetic field dependence of the thermocouple.

3.3 Specimen

The YBa$_2$Cu$_3$O$_{7-\delta}$ sample used in our measurements is a high quality twined single crystal ($\approx 2 \times 2 \times 0.4$ mm) grown from the flux. It has a superconducting transition temperature of $T_c \simeq 90.5$ K with a transition width of about $\Delta T_c \simeq 0.6$ K. This value of T_c indicates that the sample is nearly optimally doped. The resistivity and the (inverse) Hall coefficient of this sample as a function of temperature are shown in the upper panel of Figure 5.

Table 1. Selected data on the YBCO and BSCCO samples used in the present study. The values in brackets for BSCCO give results obtained for another crystal of the same batch. ρ_{xx} is the resistivity and R_H is the Hall coefficient. $k_{xx}^{\text{el},L}$ is calculated from ρ_{xx} using the Wiedemann-Franz law, i.e. $k_{xx}^{\text{el},L} = L_0 T/\rho_{xx}$. L_{xy}/L_0 is the relative Lorenz number calculated from the transverse transport coefficients according to $L_{xy}/L_0 = k_{xy}/(L_0 T\sigma_{xy})$. $k_{xx}^{\text{el},T}$ is calculated from $k_{xy}^{\text{el},T} = k_{xy}\sigma_{xx}/\sigma_{xy}$ (see Eq. (20) and Fig. 21). It should be corrected for the chain contribution. (See text.)

	T (K)	YBCO	BSCCO
ρ_{xx} ($\mu\Omega$ m)	100	2.5	10 (20)
	200	3.8	12.5 (22.5)
R_H (10^{-9} Vm/AT)	100	3.75	14
	200	1.5	9
$k_{xx}^{\text{el},L}$ (W/Km)	100	0.98	0.25 (0.125)
	150		0.3
	200	1.29	0.39 (0.22)
L_{xy}/L_0	100	1.78	2.9
	150	2.65	3.3
$k_{xx}^{\text{el},T}$ (W/Km)	100	1.8	0.75
	150	2.4	1.0
	200	3.5	

ρ_{xx} varies linearly with T in the normal state and it extrapolates to a rather low value for $T \rightarrow 0$. The absolute value of order 2.5 $\mu\Omega$ m close to T_c is rather low compared to other twinned crystals. These findings signal a good crystal quality and, in particular, that impurity scattering is weak compared to the inelastic, temperature dependent scattering processes. The linear temperature variation of the resistivity confirms that the sample is nearly optimally doped. The Hall coefficient R_H increases with decreasing temperature. The results are comparable to those of previous studies. The strong temperature dependence of R_H is characteristic for the cuprates (see Sect. 2).

The $\text{Bi}_2\text{Sr}_2\text{CaCu}_2\text{O}_{8+\delta}$ single crystals ($\approx 1 \times 1 \times 0.05$ mm) were also grown from the flux. They have a superconducting transition temperature of $T_c \simeq 80$ K, which indicates that these crystals are not optimally doped. It turned out to be difficult to remove the silver epoxy contacts used for the electrical measurements from the BSCCO samples without damaging them. We have therefore used different samples from the same batch for the electrical and thermal measurements. The resistivity and the (inverse) Hall coefficient of one of the BSCCO samples is shown in the lower panel of Figure 5. Note that the absolute value of the resistivity and the weaker temperature dependence signal that the BSCCO crystals contain significantly more defects than the YBCO crystal. An additional complication with the BSCCO crystals was that different samples from the same batch did not show the same resistivity behavior (see Tab. 1). This may be related to structural defects, microcracks, or to grain boundaries in crystals composed from several crystallites. The Hall coefficient R_H also increases with decreasing temperature.

All crystals used in our study are twined so that there is no a-b-anisotropy. We therefore set $\sigma_{xx} = \sigma_{yy}$ and $k_{xx} = k_{yy}$ in the following.
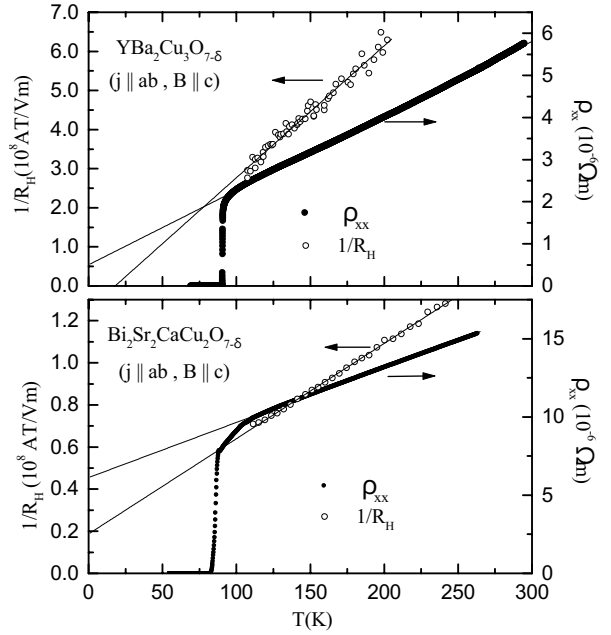

Fig. 5. In-plane resistivity ρ_{ab} (right scale) and inverse Hall coefficient $1/R_H$ (left scale) *versus* temperature of YBCO (upper panel) and BSCCO (lower panel). The straight lines are linear fits to the data used later for the extrapolation of the electrical Hall angle $\tan\alpha_H$ to temperatures $T < T_c$.

4 Test measurements on niobium

We have measured the thermal Hall effect in niobium in order to check the reliability of our experimental method. The specimen used for the measurements were 2 niobium-foils of dimensions $2 \times 4 \times 0.13$ mm^3 taken from the same sample. One specimen was used for the electrical and the other for the thermal measurements.

We show in the upper panel of Figure 6 the ratio $\tan\alpha_R \equiv \nabla_y T/\nabla_x T$ as a function of the magnetic field at various fixed temperatures. Note that in niobium the electronic contribution to the heat current is much larger than the phononic contribution and that therefore, in contrast to the cuprates, $\tan\alpha_R$ is purely electronic. As expected $\tan\alpha_R$ varies linearly with B. We have also verified that $\nabla_y T$ varies linearly with the heating power, as shown in the lower panel of Figure 6. The temperature dependence of $\tan\alpha_R$ measured at $B = 14$ T is shown in Figure 7. We find that $\tan\alpha_R$ is of order 10^{-3} in 1 T at temperatures around 100 K and one order of magnitude larger at low temperatures. It increases with decreasing temperature, as expected, since $\tan\alpha_R \propto \tau$ (see Eq. (11)) and $\tau \propto T^{-1}$ due to electron phonon scattering, consistent with the behavior of the resistivity (see inset Fig. 7).

Since $\tan\alpha_R$ is electronic we obtain from the Wiedemann Franz law (Eq. (9)) and the definition of the transport coefficients that

$$\tan\alpha_R = \frac{k_{xy}}{k_{xx}^{\text{el}}} = \frac{L_{xy}T\sigma_{xy}}{L_{xx}T\sigma_{xx}} = \frac{L_{xy}}{L_{xx}}\frac{BR_H}{\rho_{xx}}, \qquad (15)$$
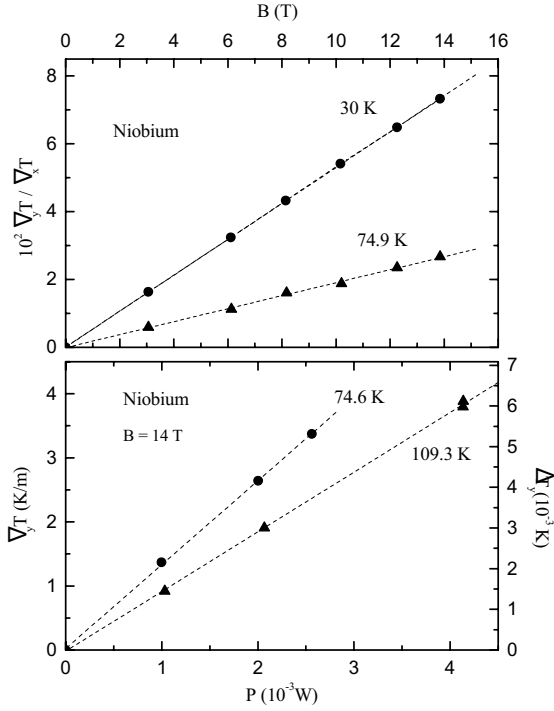
Fig. 6. Upper panel: $\nabla_y T/\nabla_x T$ of niobium *versus* magnetic field B at 30 K and 74.9 K. Lower panel: $\nabla_y T$ (left scale) and temperature difference ΔT_y (right scale) *versus* heating power P at 74.6 K and 109.3 K.
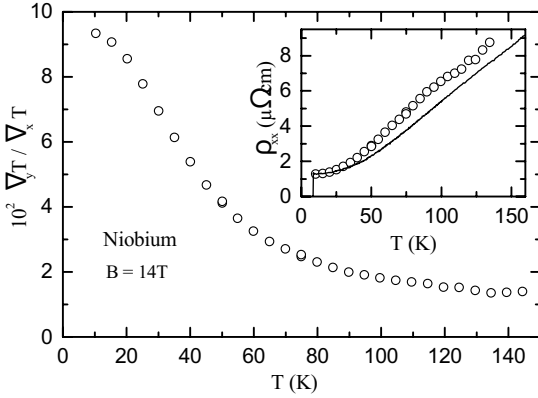

Fig. 7. Thermal Hall angle $\tan\alpha_{\mathrm{R}} = \nabla_y T/\nabla_x T$ of niobium *versus* temperature measured at $B = 14$ T. Inset: Temperature dependence of the measured electrical resistivity ρ_{xx} (full line) of niobium and of the resistivity as calculated from $R_{\mathrm{H}}(30\text{ K})$ and $\tan\alpha_{\mathrm{R}}$ according to $\rho_{xx} = BR_{\mathrm{H}}(30\text{ K})/\tan\alpha_{\mathrm{R}}$ (symbols). (See text.)

where we have used that $\sigma_{xy} \simeq BR_{\mathrm{H}}\sigma_{xx}^2$ and $\sigma_{xx} \simeq \rho_{xx}^{-1}$ in the weak field limit $\omega_c\tau \ll 1$. Here we have defined the longitudinal and transverse Lorenz numbers, L_{xx} and L_{xy}, respectively. The Wiedemann Franz law (Eq. (9)) tells that $L_{xx} = L_{xy}$. Then equation (15) leads to

$$\rho_{xx} = \frac{BR_{\mathrm{H}}}{\tan\alpha_{\mathrm{R}}} . \tag{16}$$

We compare in the inset of Figure 7 the temperature dependences of the electrical resistivity of the niobium sam-

ple and of $BR_{\mathrm{H}}(30\text{ K})/\tan\alpha_{\mathrm{R}}$, both obtained from our measurements. The agreement is very good within the experimental accuracy and demonstrates the reliability of our experimental method for determining the Righi-Leduc effect.

The deviations between ρ_{xx} and $BR_{\mathrm{H}}/\tan\alpha_{\mathrm{R}}$ at higher temperatures (see Fig. 7) may be due to a weak temperature dependence of the Hall coefficient. Alternatively, they may be due to a failure of the Wiedemann Franz law. In this case the Lorenz numbers are usually temperature dependent. It has been pointed out in reference [30] that the temperature dependencies of L_{xx} and L_{xy} may be different so that $L_{xx}(T)$ and $L_{xy}(T)$ do not cancel in equation (15). For example, inelastic scattering processes give different mean-free paths for the entropy (ℓ_S) and charge (ℓ_e) currents. In this case $L_{xx} \propto \ell_S/\ell_e$, but L_{xy}, which involves the squares of the mean free paths (see Eq. (10)), is given by $L_{xy} \propto \ell_S^2/\ell_e^2 \propto L_{xx}^2$. This is confirmed by a recent study on copper [30].

5 Experimental results

5.1 YBa$_2$Cu$_3$O$_{7-\delta}$

The thermal conductivity k_{xx} of the YBCO sample in zero magnetic field as a function of temperature is shown in the upper panel of Figure 8. k_{xx} decreases with increasing temperature in the normal state. The absolute value at T_c is of order 10 W/Km. k_{xx} increases drastically below T_c and reaches a maximum at $T_p \approx 38$ K. This behavior of k_{xx} confirms results on YBCO of previous studies [1–14]. We compare some data as found in different studies of YBCO in Table 2. This comparison reveals the following systematics: (1) The absolute value of k_{xx} at T_c does not vary strongly between different studies and is in the range of 10–15 W/Km. Twined samples are at the lower and untwined samples are at the higher end of this interval. (2) The value of k_{xx} at the peak varies much stronger. Since the largest values of k_{xx} should occur in the cleanest samples, this suggests to use the ratio $k_{xx}(T_p)/k_{xx}(T_c)$ as a measure of sample quality. (3) The peak of k_{xx} appears usually at temperatures T_p around 40 K. However, T_p is clearly sample dependent. Comparing the data with the lowest and highest values of $k_{xx}(T_p)/k_{xx}(T_c)$ reveals a weak correlation with the peak position: The peak occurs at somewhat lower temperatures in samples with a large value of $k_{xx}(T_p)/k_{xx}(T_c)$. Data on untwined crystals [11,13] indicate that the peak position is somewhat lower for the thermal conductivity along the b-direction. This maybe related to a contribution to the maximum of k_{xx} from the CuO-chains (see below and Fig. 17).

Using the Wiedemann Franz law with $L = L_0$ and the measured resistivity we find that $k_{xx}^{\mathrm{el}} = L_0 T/\rho_{xx}$ is of the order 1–2 W/Km in the normal state. We anticipate that k_{xx}^{el} obtained from the thermal Hall effect according to our data analysis (see below) is of about the same magnitude. Since $k_{xx}(T > T_c) \approx 10$ W/Km we conclude that most of the heat is carried by phonons in the normal state.

		dir.	$k_{xx}(T_c)$	$k_{xx}(T_p)$	$\frac{k_{xx}(T_p)}{k_{xx}(T_c)}$	T_p
Hagen *et al.* [2]	1	*ab*	8	9	1.1	60
	2	*ab*	8.5	12	1.4	45
Palstra *et al.* [3]		*ab*	10	11.5	1.15	60
Peacor *et al.* [5]	1	*ab*	12	19	1.6	42
	2	*ab*	14	26	1.9	42
Cohn *et al.* [8]	1	*a*	11	21	1.9	45
		b	11	18	1.6	48
	2	*a*	13	28	2.1	35
		b	13	24	1,8	35
Cohn *et al.* [9]	1	*ab*	10	14.5	1.5	45
	2	*ab*	9.5	13.5	1.4	45
	3	*ab*	9	10.5	1.2	50
Yu *et al.* [7]	1	*a*	12	24	2.0	45
		b	16	29	1.8	45
Takenaka *et al.* [12]	1	*ab*	16	32	2.0	40
Aubin *et al.* [13]	1	*b*	11	27	2.2	23
Krishana *et al.* [26]	1	*ab*	16	27	1.7	40
Gagnon *et al.* [11]	1	*a*	11	25	2.3	37
		b	14	33	2.4	30
Zeini *et al.* (this work)	1		10.5	16.5	1.6	38

Table 2. Selected experimental data on the thermal conductivity k_{xx} of single crystals of YBCO (close to optimum doping) given in W/Km. The first column lists the number of different crystals studied. The second column refers to the crystalline direction: *ab*: within the CuO$_2$-planes in a twined crystal; *a*, *b*: along the *a*- and *b*-direction, respectively. The CuO-chains are along the *b*-direction. $k_{xx}(T_c)$ and $k_{xx}(T_p)$ are the values of k_{xx} at T_c and at the maximum, respectively, and T_p is the position of the maximum given in K.
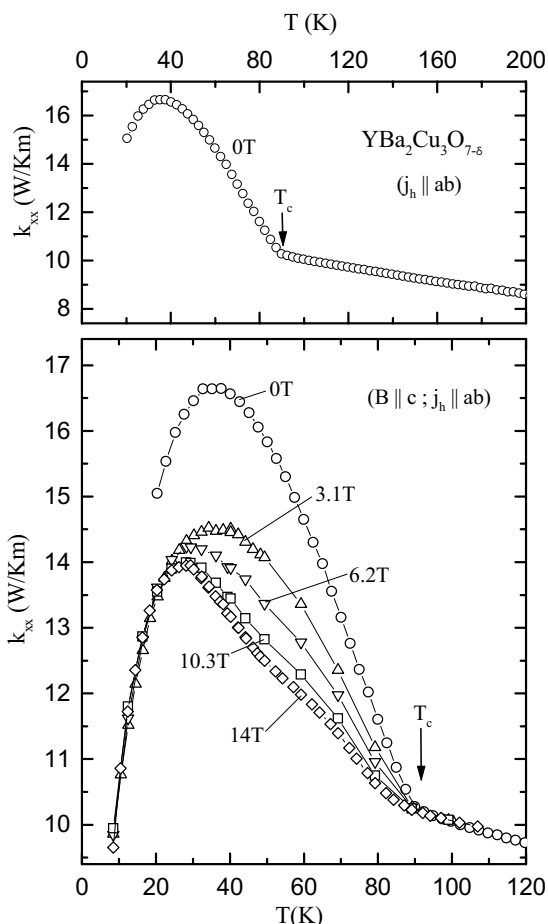

Fig. 8. Upper panel: Zero field thermal conductivity k_{xx} of YBCO as a function of temperature. Lower panel: k_{xx} of YBCO as a function of temperature measured at various fixed magnetic fields indicated in the figure. Note the different temperature scales of the upper and lower panel.

The normal state thermal conductivity is independent of the magnetic field within our experimental resolution. In contrast, k_{xx} is strongly suppressed by a magnetic field below T_c as shown in Figure 8. This confirms results on YBCO of previous studies [3–5,10,14]. The magnetic field dependence of k_{xx} is shown in Figure 9, where we plot $\Delta k_{xx} = k_{xx}(B) - k_{xx}(B = 0)$ as a function of the magnetic field at fixed temperatures. k_{xx} varies non-linearly with B, and the magnetic field dependence changes with temperature: At the lowest temperatures measured, k_{xx} has a tendency to become magnetic field independent at high fields. This is reminiscent of the behavior reported recently by Krishana *et al.* for BSCCO [50].

k_{xy} *versus* temperature at $T > T_c$ is shown in the upper panel of Figure 10. k_{xy} is positive and of order 10^{-2} W/Km for $B \approx 1$ T. Comparing this to $k_{xx}(T_c) \approx 10$ W/Km reveals that k_{xy}/k_{xx} at 1 T is of the order 10^{-3}. Since k_{xx} is to a great extent due to phonons the thermal Hall angle $\tan \alpha_H = k_{xy}/k_{xx}^{el}$ cannot be calculated quantitatively at his point. $k_{xy}(T > T_c)$ decreases with increasing temperature, approximately like $k_{xy} \propto T^{-p}$ with $1 < p < 2$. A distinction between $p = 1$ and $p = 2$ cannot be inferred from the data of Figure 10 because of the limited temperature interval. Below T_c k_{xy} exhibits a pronounced maximum, as shown in the lower panel of Figure 10. The position of this maximum shifts slightly to higher temperatures with increasing magnetic field from about 40 K at $B = 3$ T to nearly 50 K at $B = 14$ T. At first glance the behavior of k_{xy} is rather similar to that of k_{xx}. However, a more thorough comparison of the data shows that the maximum of k_{xy} occurs at a higher temperature and that its relative increase below T_c is much larger.

The magnetic field dependence of k_{xy} is shown in Figure 11. Above T_c, k_{xy} increases linearly with B, as expected in the weak field limit (see Eq. (10)). In contrast,
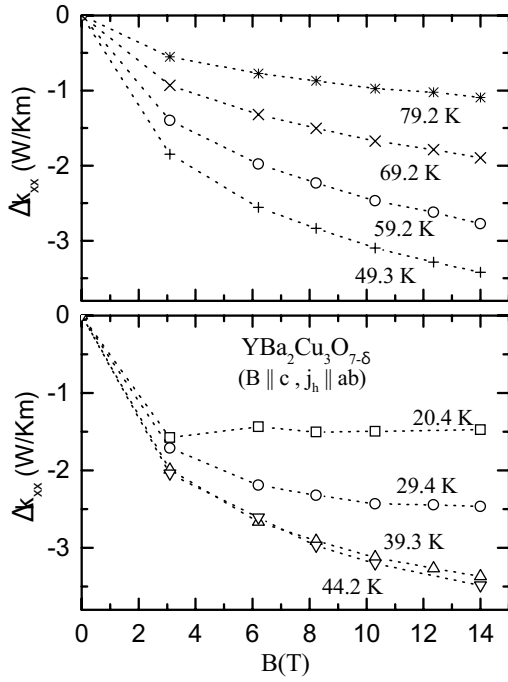
Fig. 9. $\Delta k_{xx} = k_{xx}(B) - k_{xx}(B=0)$ of YBCO as a function of the magnetic field B at various fixed temperatures given in the figure.
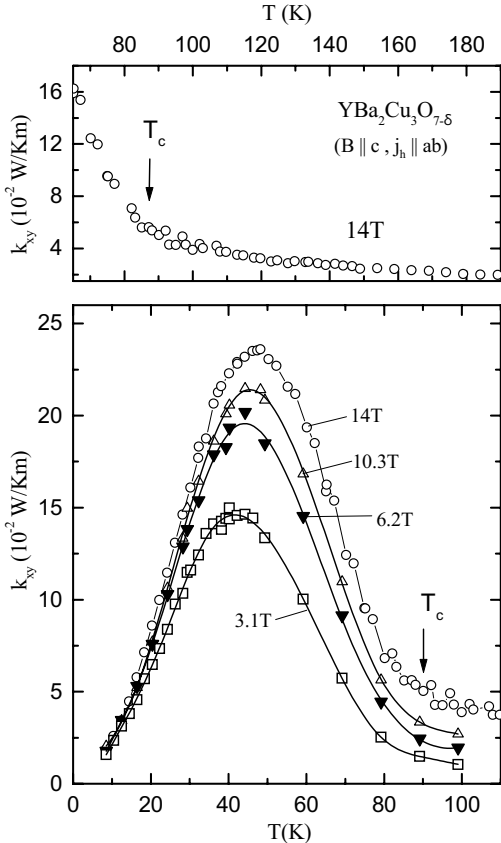

Fig. 10. Upper panel: Transverse thermal conductivity k_{xy} of YBCO as a function of temperature in the normal state measured at $B = 14$ T. Lower panel: k_{xy} of YBCO as a function of temperature at various fixed magnetic fields given in the figure. Note the different temperature scales of the upper and lower panel.
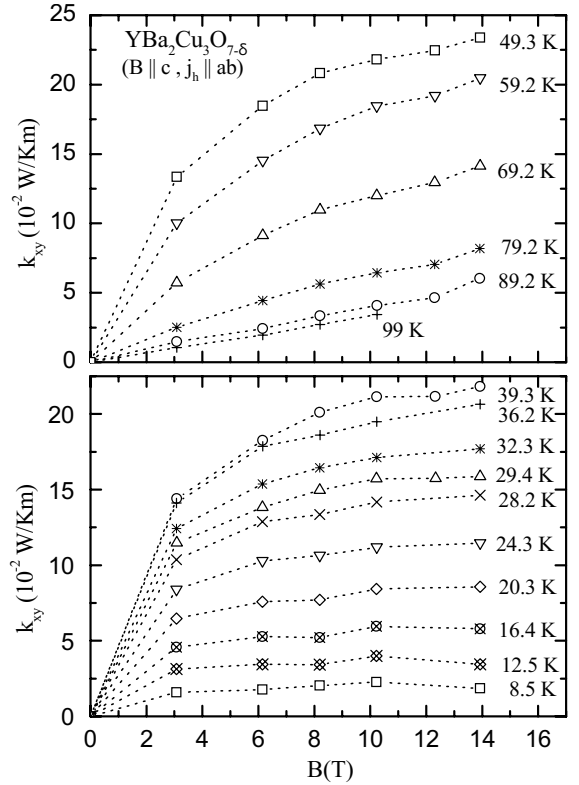

Fig. 11. Transverse thermal conductivity k_{xy} of YBCO as a function of magnetic field for various fixed temperatures given in the figure.

below T_c the magnetic field dependence of k_{xy} changes from $k_{xy} \propto B$ near T_c to non-linear behavior at low temperatures. At the lowest measured temperatures k_{xy} has a tendency to become independent of B at high magnetic fields above 3 T. We note that the data of Figure 11 are similar to the results of a previous study [26]. On the other hand, we do not find a decrease of k_{xy} with B at high magnetic fields, in contrast to what is reported in reference [51].

5.2 Bi$_2$Sr$_2$CaCu$_2$O$_{8+\delta}$

The longitudinal thermal conductivity k_{xx} of BSCCO is shown as a function of temperature in the upper panel of Figure 12. k_{xx} is magnetic field independent in the normal state. In contrast to YBCO it increases slightly with temperature. k_{xx} is of order 3 W/Km near T_c, significantly smaller than the value found in YBCO. Using the data of Table 1 we find that $k_{xx}^{\mathrm{el}} = L_0 T/\rho_{xx}$ is of the order of 0.3 W/Km. Comparing this to the total thermal conductivity reveals that also in BSCCO most of the heat is carried by phonons in the normal state. Below T_c in zero field a weak upturn of k_{xx} occurs with a maximum around 70 K. This maximum is almost completely suppressed when applying a magnetic field of 14 T.

$k_{xy}(T)$ measured on this sample is shown in the lower panel of Figure 12. The behavior of k_{xy} is qualitatively similar to that found in YBCO. In particular, although
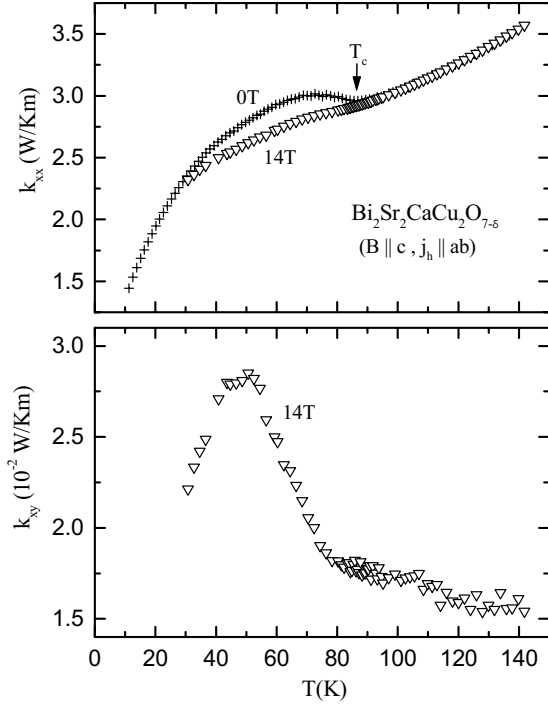
Fig. 12. Upper panel: Thermal conductivity k_{xx} of BSCCO as a function of temperature in zero field (full symbols) and $B = 14$ T (open symbols). Lower panel: k_{xy} of BSCCO as a function of temperature measured at $B = 14$ T.
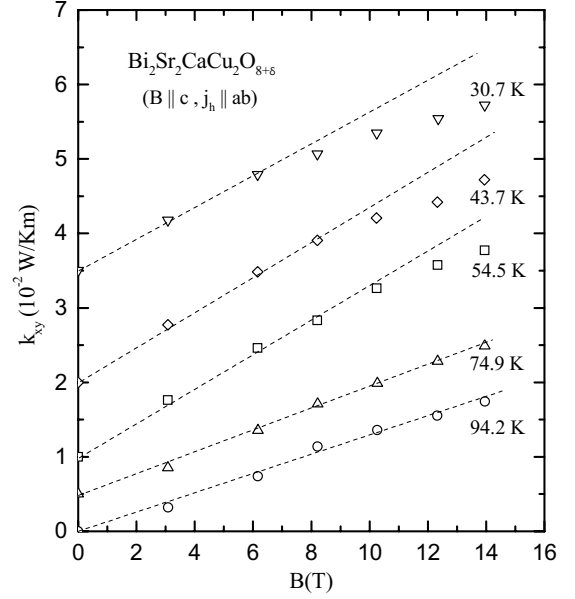

Fig. 13. Transverse thermal conductivity k_{xy} of BSCCO as a function of magnetic field at various fixed temperatures given in the figure. For clarity the curves have been shifted by a value given by the intersection of the dotted lines (*i.e.* $k_{xy} = 0$ for all curves). The dotted lines $\propto B$ are a guide to the eye in order to indicate the deviations from linearity at high magnetic fields and low temperatures.

the maximum of k_{xx} below T_c is hardly visible in BSCCO, k_{xy} clearly shows a pronounced maximum at about 50 K. Note that in comparison to YBCO in BSCCO the absolute magnitude of $k_{xy}(14\text{T})$ is smaller by a factor of about 4 in the normal state close to T_c and by a factor of about 10 at the maximum.

A further clear difference to YBCO is apparent when inspecting the magnetic field dependence of k_{xy} in BSCCO, which is shown in Figure 13. In the normal state $k_{xy} \propto B$, as in YBCO. However, below T_c k_{xy} still varies approximately linearly with B. Weak non-linearity occurs only at low temperatures and high magnetic fields.

6 Data analysis

6.1 Contributions to the heat current

We assume that k_{xx} is the sum of 3 contributions:

$$k_{xx} = k_{xx}^{\text{el}} + k_{xx}^{\text{ch}} + k_{xx}^{\text{ph}} = k_{xx}^{\text{el}} + k_{xx}^{\text{rest}}. \qquad (17)$$

Here k_{xx}^{el} is the electronic thermal conductivity of the CuO$_2$-planes (in fact, bilayers in YBCO and BSCCO) and k_{xx}^{ph} is the phononic thermal conductivity. k_{xx}^{ch} is an optional contribution. It must be included in the data analysis only if an additional electronic channel of heat conduction is present with a magnetic field or temperature dependence *different* from that of k_{xx}^{el}. Such a situation is most probably realized in YBCO, where in addition to

the CuO$_2$-planes (pl) common to all HTSCs CuO-chains (ch) are present along the b-direction of the orthorhombic crystal structure. In good untwined crystals these chains lead to a rather strong a-b anisotropy of the electronic properties. For example, the anisotropy of the electrical conductivity is of order 2, suggesting that along the b-direction $\sigma_{xx}^{\text{ch}} \approx \sigma_{xx}^{\text{pl}}$ [31–33]. (Note that in order to avoid confusion we keep the notation as appropriate for twined crystals with $\sigma_{xx} = \sigma_{yy}$ and $k_{xx} = k_{yy}$ and denote the chain contribution by (ch).) Similarly, as expected from the Wiedemann-Franz law, a large contribution of the CuO-chains to the heat conductivity has also been established experimentally [7,11]. Note that a contribution of the chains to σ_{xx} and k_{xx} occurs even for twined samples as an in-plane average of σ_{xx}^{ch} and k_{xx}^{ch}. Since the CuO-chains are a one-dimensional channel of conduction the magnetic field and temperature dependence of k_{xx}^{ch} may be different from that of k_{xx}^{el}. In particular, we expect no magnetic field dependence of k_{xx}^{ch}. Moreover, due to their one-dimensionality the CuO-chains should also not contribute to the transverse effects, *i.e.* to k_{xy} and σ_{xy}.

In the normal state only the above contributions to the heat current are relevant in optimally doped cuprates. In contrast, below T_c in finite magnetic fields an additional heat current arises from the motion of vortices [35,36]. The contribution k_{xy}^{v} of this heat current to the thermal Hall effect has been calculated in reference [37]. It is given by

$$k_{xy}^{\text{v}} = -\frac{s_{\text{v}}}{\Phi_0} ST. \qquad (18)$$

Here, s_{v} is the transport entropy of a vortex (per unit length). It is usually obtained from measurements of the Nernst effect (or the Ettingshausen effect) and the flux-flow resistivity [3,25,35,52–55]. Φ_0 is the flux quantum and S is the thermopower (or Seebeck-coefficient) [25,35,53–55]. For an estimate we use the data on YBCO of references [54,55]: $s_{\mathrm{v}} \approx 5 \times 10^{-15}$ J/Km close to $T_{\mathrm{c}} \approx 90$ K and $S(T_{\mathrm{c}}) \approx 2.5$ μV/K. This yields $k_{xy}^{\mathrm{v}}(T_{\mathrm{c}}) \approx -5 \times 10^{-4}$ W/Km. A calculation using the temperature dependencies of s_{v} and of S shows that $|k_{xy}^{\mathrm{v}}|$ increases with decreasing temperature below T_{c} and reaches a maximum at about 80 K [37]. At the maximum $|k_{xy}^{\mathrm{v}}|$ is of the order 2×10^{-3} W/Km, which is about two orders of magnitude smaller than the measured values of k_{xy} in YBCO (compare Fig. 10). Thus, the vortex contribution to k_{xy} is by far too small to be relevant for our results and can safely be neglected in the following. We note that there is also no anomaly of k_{xy} around the irreversibility line, confirming that k_{xy}^{v} does not give a sizeable contribution to k_{xy}. The contribution of the vortices to the longitudinal heat current and thus to k_{xx} is of the same magnitude as k_{xy}^{v} and therefore negligible [37].

For completeness we mention the so called circulatory contribution k_{xx}^{c} to the heat current (see *e.g.* Ref. [1]) which occurs in superconductors. It is given by $k_{xx}^{\mathrm{c}} = S^2 T / \rho_{xx}$. Using $\rho_{xx}(T_{\mathrm{c}}) \approx 2\mu\Omega\,\mathrm{m}$ we find $k_{xx}^{\mathrm{c}} \approx 5 \times 10^{-3}$ W/Km, much smaller than the experimental values for single crystals.

6.2 Separation of the electronic and phononic heat currents

6.2.1 Wiedemann-Franz law

The electronic and phononic thermal conductivity are often separated using the Wiedemann-Franz law. On this basis, if transverse transport phenomena are involved, there are two ways to determine k_{xx}^{el}: k_{xx}^{el} may be calculated directly from the electrical conductivity σ_{xx} according to

$$k_{xx}^{\mathrm{el}} = L_0 T \sigma_{xx}. \tag{19}$$

Here one assumes that the Lorenz-number is a constant, which is often not the case, in particular when inelastic scattering processes are important. Alternatively we may extract k_{xx}^{el} from the normal state electrical Hall angle and from k_{xy}, according to

$$k_{xx}^{\mathrm{el}} = \frac{k_{xy}}{\tan \alpha_{\mathrm{R}}} = \frac{k_{xy}}{\tan \alpha_{\mathrm{H}}} = k_{xy} \frac{\sigma_{xx}}{\sigma_{xy}}. \tag{20}$$

One may expect that this latter method is more general than the direct calculation from the resistivity since it does not require the validity of the Wiedemann Franz law, but only that $L_{xx}(T) = L_{xy}(T)$. (Compare, however, Eq. (15) and the corresponding discussion.)

In the superconducting state both methods to determine k_{xx}^{el} cannot be used in a straightforward way.

The first method requires knowledge of the QP conductivity. To obtain σ_{xx} the superfluid response to electric fields must be separated from that of the QPs, which requires a (model dependent) analysis [15]. Moreover, the Wiedemann-Franz law itself is not necessarily fulfilled in the superconducting state even for elastic scattering [20]. The second method suffers from the lack of knowledge of the Hall angle below T_{c}. In addition to the QP conductivity knowledge of the Hall angle requires a measurement of the QP Hall effect. Again the superfluid and vortex contributions to the Hall effect would have to be separated from that of the QPs, which is difficult, in particular in view of the current incomplete understanding of the Hall effect in the superconducting state [35].

6.2.2 Thermomagnetic separation

To avoid these difficulties we present in the following a different route towards a separation of the electronic and phononic channels of heat conduction, which is based on the results for k_{xy} and the magnetic field dependence of k_{xx}. This method does not rely on the validity of the Wiedemann-Franz law.

We relate the transverse and longitudinal electronic thermal conductivity (of the CuO$_2$-planes) according to

$$k_{xy} = k_{xx}^{\mathrm{el}} \tan \alpha_{\mathrm{R}} = k_{xx}^{\mathrm{el}} \omega_{\mathrm{c}} \tau_{\mathrm{R}}. \tag{21}$$

We assume here, as discussed above, that the chains do not contribute to k_{xy}. Equation (21) defines a relaxation time $\tau_{\mathrm{R}}(T, B)$, which is used to parameterize the temperature and magnetic field dependence of the thermal Hall angle. The distinction between τ and τ_{R} is of course motivated by the distinction between τ and τ_{H} necessary in the normal state for the electrical transport properties. Nevertheless, we leave open at this point whether τ_{R} must be identified with the transport or the Hall relaxation time (and whether a distinction of two relaxation times is necessary at all).

The key experimental observation underlying the analysis is that $\Delta k_{xx} = k_{xx}(B) - k_{xx}(B=0)$ and k_{xy}/B have the same magnetic field dependence, *i.e.*

$$\frac{\partial}{\partial B}\left(\frac{k_{xy}}{B}\right) \propto \frac{\partial k_{xx}}{\partial B}. \tag{22}$$

This is shown in Figure 14. Since k_{xy} is purely electronic, the only reasonable interpretation of this finding is that the magnetic field dependence of k_{xx} is entirely due to that of k_{xx}^{el}. This may be seen by noting that

$$\frac{m}{e} \frac{\partial}{\partial B}\left(\frac{k_{xy}}{B}\right) = \tau_{\mathrm{R}} \frac{\partial k_{xx}^{\mathrm{el}}}{\partial B} + k_{xx}^{\mathrm{el}} \frac{\partial \tau_{\mathrm{R}}}{\partial B} =$$
$$\tau_{\mathrm{R}} \frac{\partial k_{xx}}{\partial B} + k_{xx}^{\mathrm{el}} \frac{\partial \tau_{\mathrm{R}}}{\partial B} - \tau_{\mathrm{R}} \frac{\partial k_{xx}^{\mathrm{ph}}}{\partial B} - \tau_{\mathrm{R}} \frac{\partial k_{xx}^{\mathrm{ch}}}{\partial B} \tag{23}$$

by equations (21) and (17). Obviously, our experimental results (Eq. (22)) suggest that the term in brackets vanishes. Since the 3 terms in brackets refer to 3 different
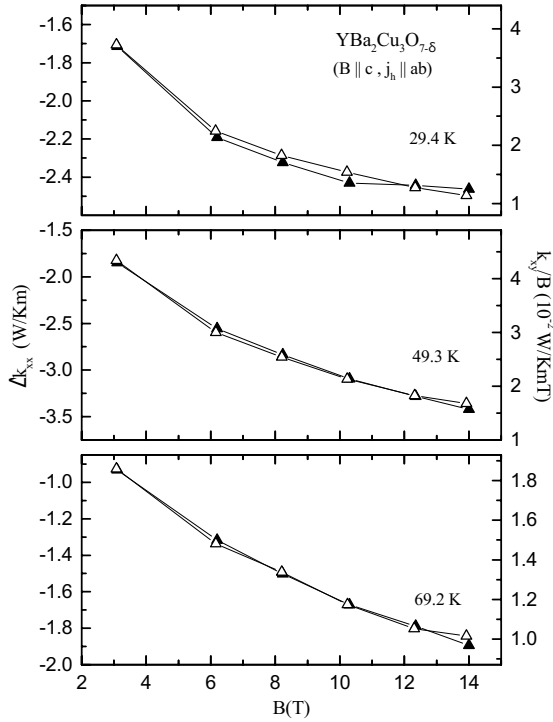
Fig. 14. $\Delta k_{xx} = k_{xx}(B) - k_{xx}(B=0)$ (full symbols, left scale) and k_{xy}/B (open symbols, right scale) of YBCO as a function of magnetic field for various fixed temperatures given in the figure.

channels of heat conduction this requires that τ_R, k_{xx}^{ph}, and k_{xx}^{ch} are separately field independent so that indeed

$$\frac{\partial k_{xx}}{\partial B} \simeq \frac{\partial k_{xx}^{el}}{\partial B}, \qquad (24)$$

as stated above. We emphasize that this conclusion is rather natural: k_{xx}^{ph} and k_{xx}^{ch} should apparently be field independent. The Hall relaxation time τ_H is known to be field independent in the normal state. With these results and using equation (23), τ_R may be determined from equation (21) according to

$$\frac{e}{m}\tau_R = \frac{\partial}{\partial B}\frac{k_{xy}}{B} \Big/ \frac{\partial k_{xx}}{\partial B} = \frac{\Delta(k_{xy}/B)}{\Delta k_{xx}}$$
$$= \frac{k_{xy}(B_1)/B_1 - k_{xy}(B_2)/B_2}{k_{xx}(B_1) - k_{xx}(B_2)}. \qquad (25)$$

Once τ_R is known the remainder of our analysis is straightforward:

1. $k_{xx}^{el}(B \neq 0)$ follows from equation (21) according to

$$k_{xx}^{el}(B,T) = \frac{k_{xy}(B,T)}{\omega_c \tau_R(T)} \qquad (26)$$

 using our data for $k_{xy}(B)$.

2. k_{xx}^{rest} is subsequently obtained from equation (17) according to

$$k_{xx}^{rest}(T) = k_{xx}(B,T) - k_{xx}^{el}(B,T) \qquad (27)$$

using $k_{xx}(B)$ and $k_{xx}^{el}(B)$ at finite magnetic fields. Note that internal consistency of our analysis requires that k_{xx}^{rest} is field independent.

3. The zero field thermal conductivity $k_{xx}(B=0)$ follows from equation (17) according to

$$k_{xx}^{el}(B=0,T) = k_{xx}(B=0,T) - k_{xx}^{rest}(T) \qquad (28)$$

using the zero field data for k_{xx}. As another check for internal consistency, $k_{xx}(B=0)$ may also be determined directly from equation (21) by extrapolating B/k_{xy} to $B=0$.

The results of this data analysis will be shown and discussed in the next section.

7 Discussion

7.1 General conclusions

Several conclusions can be drawn from our experimental results already without a detailed data analysis. First of all, our experiments clearly demonstrate that the electronic quantity k_{xy} increases strongly below T_c in YBCO and in BSCCO. Since the superfluid does not transport heat and since the vortex contribution to k_{xy} is negligibly small, this increase must be due to an increase of the QP contribution to k_{xy}. Since the number (density) n_{QP} of QPs decreases with decreasing temperature below T_c the increase of k_{xy} requires that the QP relaxation time increases below T_c so strongly that the decrease of n_{QP} is overcompensated. This conclusion holds irrespective of whether $k_{xy} \propto \tau^2$ as in conventional metals or whether $k_{xy} \propto \tau \tau_H$. It also does not rely on the validity of the Wiedemann Franz law. The strong increase of τ below T_c provides strong evidence for an electronic origin of the in-plane scattering processes: If electron phonon scattering was the main source of scattering, the phononic thermal conductivity would increase below T_c, but not the electronic one. In particular, the mean free path of the QPs would not be strongly enhanced below T_c. We note that our findings are in agreement with the results of photoemission studies, which reveal well defined QPs below T_c in contrast to the strongly damped excitations of the normal state [57,58]. Thus, the existence of well defined QPs below T_c as inferred from photoemission, microwave conductivity and thermal conductivity receives direct and unambiguous confirmation from the thermal Hall effect.

A further important observation is that the upturn of k_{xy} is found in both, YBCO and BSCCO. This suggests that the corresponding increase of the relaxation time is a generic feature of the cuprates. The much weaker overall enhancement in BSCCO compared to YBCO must then be attributed to the stronger impurity scattering in BSCCO, which sets a cutoff to the increase of the relaxation time.

7.2 Electronic heat transport in the CuO$_2$-planes

In this section we describe in detail the results of the data analysis discussed above. The thermomagnetic separation

crucially exploits the magnetic field dependence of k_{xx}. It is therefore applicable only below T_c (and above about 20–30 K), where k_{xx} is magnetic field dependent, and it is reliable only for YBCO, since in BSCCO the field dependence of k_{xx} is weak. Therefore we concentrate in this section on YBCO.

7.2.1 Hall angle

The thermal Hall relaxation time τ_R as obtained from our data below T_c using equation (25) is shown in Figure 15. The values obtained for different magnetic fields coincide within the experimental accuracy, consistent with τ_R being magnetic field independent. The field independence of τ_R is compatible with the normal state behavior of the Hall relaxation time τ_H, which is also found to be B-independent. Note that the error in τ_R increases below 30 K, since k_{xx} hardly depends on the magnetic field in this regime and therefore the data analysis becomes difficult.

As a check of our result for τ_R we have also determined $\tau_H = \omega_c^{-1} \sigma_{xy}/\sigma_{xx}$ for the same sample from measurements of σ_{xy} and σ_{xx} in the normal state. We have extrapolated the normal state data to temperatures below T_c by using linear fits to ρ_{xx} and R_H^{-1} separately, which vary linearly with temperature with high accuracy (see Fig. 5). Subsequently the electrical Hall angle below T_c has been calculated from these fit functions. The result of this extrapolation is also shown in Figure 15. Remarkably, τ_R and τ_H have the same temperature dependence, given by $\tau_R^{-1} \propto \tau_H^{-1} \propto T^2$.

Regarding the absolute values, τ_R appears to be larger than τ_H by roughly a factor of order 2 (see Fig. 15). However, this discrepancy can be explained by taking into account the presence of CuO-chains: τ_R as extracted from the thermal transport data is clearly unaffected by the presence of the CuO-chains since only k_{xy} and the *magnetic field dependence* of k_{xx} enter. σ_{xy} is obviously also unaffected by the CuO-chains. In contrast, σ_{xx} does have a contribution from the CuO-chains, *i.e.*

$$\sigma_{xx} = \sigma_{xx}^{\mathrm{pl}} + \langle \sigma_{xx}^{\mathrm{ch}} \rangle, \qquad (29)$$

where $\sigma_{xx}^{\mathrm{pl}}$ is the electrical conductivity of the CuO$_2$-planes and $\langle \sigma_{xx}^{\mathrm{ch}} \rangle$ is an average of the chain contribution appropriate for a twined crystal. With $\sigma_{xx}^{\mathrm{pl}} \approx \langle \sigma_{xx}^{\mathrm{ch}} \rangle$ [33] we conclude that

$$\frac{e\tau_H}{m} = \frac{1}{B}\frac{\sigma_{xy}}{\sigma_{xx}} = \frac{1}{B}\frac{\sigma_{xy}}{\sigma_{xx}^{\mathrm{pl}} + \langle \sigma_{xx}^{\mathrm{ch}} \rangle} \qquad (30)$$

is underestimated by a factor of order 2 compared to τ_R. Correcting the normal state data for this factor we find excellent agreement between τ_H and τ_R, both regarding the temperature dependence as well as the absolute values, *i.e.* our data tell $\tau_R \simeq \tau_H$. A similar conclusion based on a different analysis of the thermal Hall effect in YBCO has recently been reported by Zhang *et al.* [50]. Note that the result $\tau_R \simeq \tau_H$ strongly supports the procedure of our
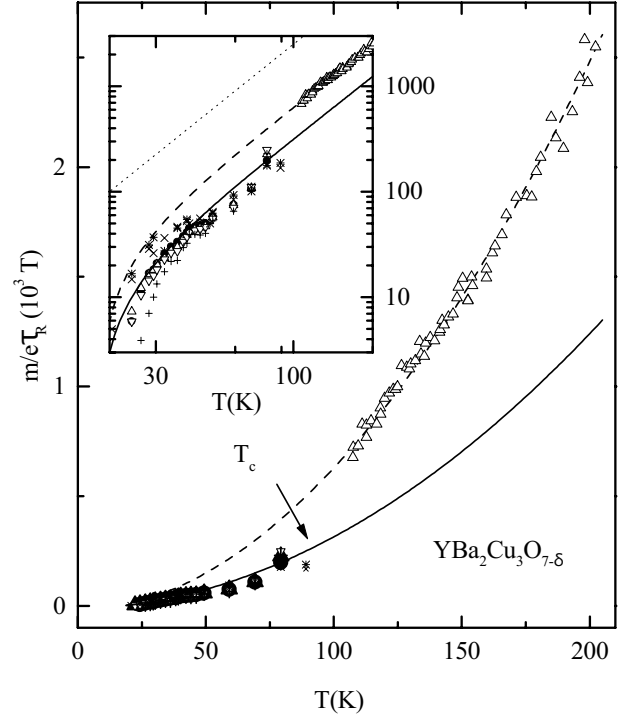

Fig. 15. $m/e\tau_R$ *vs.* temperature. $T < T_c$: Data obtained from equation (25). Different symbols correspond to different values of B_1 and B_2. $T > T_c$: $m/e\tau_H$ obtained from σ_{xy} and σ_{xx}. Dashed line: extrapolated normal state data. Solid line: extrapolated normal state data divided by a factor 2 (see text). Inset: The same data on a double logarithmic scale. The solid and dashed lines are identical with the ones in the main figure. The dotted line corresponds to $\tau_R^{-1} \propto T^2$. The deviation of the extrapolated Hall relaxation rate from a T^2-behavior at low temperatures is a result of our extrapolation procedure, in which ρ and R_H^{-1} have both been fitted by straight lines.

data analysis. Since $\tau_R \simeq \tau_H$ we shall no longer distinguish between τ_R and τ_H in the following.

Based on an analysis of vortex motion and scattering of QPs on vortices Harris *et al.* [60] have reached the conclusion that the Hall conductivity σ_{xy} shows a dramatic change below T_c. This is not in contradiction to our results, since $\sigma_{xy} \propto \tau \tau_H$ so that the strong increase of σ_{xy} below T_c results from τ (see below). No direct information on the behavior of τ_H itself is obtained from their analysis.

7.2.2 Electronic thermal conductivity

As a result of our data analysis we show in Figure 16 $k_{xx}^{\mathrm{el}}(B,T)$. Note that the zero field thermal conductivity as obtained from the extrapolation of B/k_{xy} to $B = 0$ (full symbols) corresponds well to the result extracted from equation (28) (open symbols). The extrapolation of B/k_{xy} to $B = 0$ is in fact straightforward, since B/k_{xy} varies linearly with B as shown below (see Figs. 18 and 19). Our results confirm explicitly the interpretation inferred previously from various indirect experimental probes that k_{xx}^{el} is strongly enhanced below T_c. Our result for k_{xx}^{el} is also
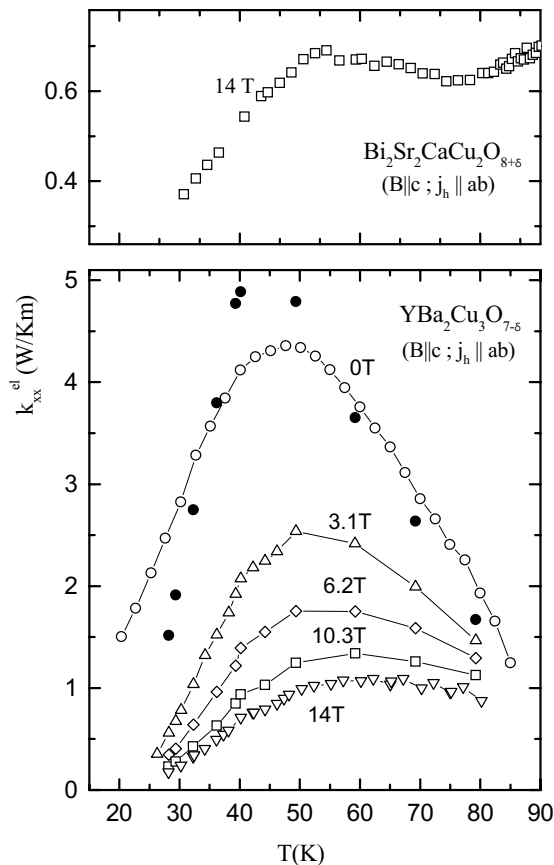
202

Fig. 16. k_{xx}^{el} as a function of temperature for various fixed magnetic fields given in the figure. Upper panel: BSCCO. Lower panel: YBCO. Full symbols: Extrapolation from B/k_{xy} to $B = 0$ (see text).

in good agreement with theoretical calculations [59]. The overall magnitude of k_{xx}^{el} near T_c is of order 1–1.5 W/Km in YBCO and of order 0.6 W/Km in BSCCO. Comparing this with the total thermal conductivity tells that k_{xx} is dominated by the phononic contribution in the normal state.

The implications of the increase of k_{xx}^{el} below T_c are straightforward. According to standard transport theory $k_{xx}^{el} \propto T n_{QP} \tau$. Regardless of the precise form of the superconducting order parameter, the number density n_{QP} of QPs decreases with decreasing temperature below T_c so that τ must increase strongly with decreasing temperature in order to overcompensate the decrease of n_{QP}.

Based on measurements of the thermal Hall effect Krishana *et al.* have previously determined the (zero field) electronic thermal conductivity of the CuO$_2$-planes in YBCO [26]. Their analysis exploits the (asymmetric) scattering of QPs on vortices as calculated by Cleary [61] as well as a variational treatment of the Boltzmann-equation for the QPs. Their results for the zero field thermal conductivity of the CuO$_2$-planes are similar to ours.

7.2.3 Two relaxation times below T$_c$

It is certainly very remarkable that τ_H remains field independent below T_c and has the same temperature dependence as above T_c, whereas τ is strongly enhanced below T_c and magnetic field dependent (see below). This should provide important information for the theoretical understanding of the transport phenomena in the cuprates. We therefore discuss this issue in some more detail here.

Proposals for the different temperature dependencies of $\tau \propto T^{-1}$ and $\tau_H \propto T^{-2}$ have invoked quite different scenarios for the characteristics of the charge carriers. These approaches range from conventional Fermi liquid like quasiparticles to more exotic spin-charge separated entities [40], and fermionic currents with well defined charge conjugation symmetry [41,42]. A common feature of Fermi liquid like theories is the necessity of an electronic scattering mechanism which leads to a highly anisotropic scattering rate for different momenta on the Fermi surface [43–48]. In these theories the terminology of *hot spots* and *cold spots* has been introduced for those regions on the Fermi surface where the scattering rate is largest or smallest, respectively. Hot spots arise due to scattering processes from antiferromagnetic spin fluctuations with large momentum transfer $\mathbf{q} \sim \mathbf{Q} = (\pi, \pi)$. Electrons on regions of the Fermi surface which are connected by $\mathbf{Q}$ thereby suffer the strongest magnetic scattering and thus acquire the shortest lifetime. For the Fermi surfaces of cuprate superconductors these hot regions are located near $(0, \pi)$ and the equivalent points in the Brillouin zone. The cold spots, *i.e.* the regions of the Fermi surface with the longest electronic lifetimes, are located instead near the Fermi surface crossing along the Brillouin zone diagonal. In particular in the cold spots models it has been argued that it is the long lived quasiparticles alone which determine the transport properties [47,49]. Ioffe and Millis [47] pointed out that a conventional Fermi liquid like T^2 dependence of the the electronic relaxation rate combined with phase restrictions to the cold Fermi surface regions explains simultaneously the T^2 temperature dependence of the Hall angle as well as the linear T dependence for the relaxation rate in the longitudinal conductivity (see below).

None of the above mentioned theories has so far been extended to the superconducting state. It appears, however, that the cold spots model is a natural candidate theory for explaining the continuing T^2 dependence of the Hall relaxation time when passing through T_c as concluded from the analysis of our thermal conductivity data. This is because the $d_{x^2-y^2}$ gap symmetry allows for gapless excitations along the nodal directions, *i.e.* along the Brillouin zone diagonals passing through the cold spots. Inspecting the model of Ioffe and Millis [47] in more detail we note that their QP-scattering rate Γ is given by

$$\Gamma(\Theta, T) = \frac{1}{4}\Gamma_0 \sin^2(2\Theta) + \frac{1}{\tau_{FL}} \cdot \quad (31)$$

Here Θ parameterizes the direction in $\mathbf{k}$-space with $\Theta = 0$ for $\mathbf{k}$ along (π, π). $\tau_{FL}^{-1} \propto T^2$ is a Fermi-liquid like scattering rate relevant for the QPs in the direction along the

Brillouin zone diagonal. Γ_0 is an anomalous temperature independent scattering rate, active at all other parts of the Fermi surface. The dc-resistivity and Hall effect in this model are given by

$$\sigma_{xx} \propto \sqrt{\frac{\tau_{\mathrm{FL}}}{\Gamma_0}} \quad \text{and} \quad \tan\alpha_{\mathrm{H}} \propto \omega_{\mathrm{c}}\tau_{\mathrm{FL}}. \qquad (32)$$

Obviously, the Hall angle is unaffected when a $d_{x^2-y^2}$-gap opens below T_{c}. On the other hand, in order to obtain a strong increase of the transport scattering time $\tau \propto \sigma_{xx} \propto \sqrt{\tau_{\mathrm{FL}}/\Gamma_0}$ below T_{c} one has to assume that Γ_0 collapses below T_{c}. This implies well defined QPs in these directions below T_{c}, which indeed have been observed in photoemission studies [58].

We finally comment on a theory by Coleman *et al.* [41,42], who have proposed that the need to distinguish two relaxation times in the cuprates may be understood in terms of scattering processes which discriminate between currents that are even or odd under charge conjugation. In their model $k_{xx}^{\mathrm{el}} \propto \tau_{\mathrm{H}}$ (!), whereas $\tan\alpha_{\mathrm{R}} = \omega_{\mathrm{c}}\tau$, *i.e.* the role of τ and τ_{H} are interchanged for the thermal transport effects. For the electrical transport properties they still find $\sigma_{xx} \propto \tau$ and $\tan\alpha_{\mathrm{H}} \propto \tau_{\mathrm{H}}$. However, note that in our data analysis we may replace $\tau \to \tau_{\mathrm{H}}$ and $\tau_{\mathrm{H}} \to \tau$ in equation (21) and we would come to the same conclusions but with the role of τ and τ_{H} interchanged. In particular, our analysis would give that the behavior of τ below T_{c} is that shown in Figure 15. This is, however, clearly in disagreement to the observation that these data agree well with the extrapolated values of the Hall angle extracted from the electrical transport data above T_{c}. Therefore, our data are not in favor of the results by Coleman *et al.* Nevertheless, a more detailed analysis of the temperature dependence of k_{xy} in the normal state should shed more light on this issue.

7.3 Chain and phonon contributions to k_{xx}

k_{xx}^{rest} as obtained from our analysis is shown in Figure 17. We find that k_{xx}^{rest} is indeed independent of the magnetic field, consistent with our conclusion that both, k_{xx}^{ch} and k_{xx}^{ph} are magnetic field independent. k_{xx}^{rest} shows a pronounced maximum below T_{c}, too. It is not possible to attribute this maximum unambiguously to k_{xx}^{ph} or to k_{xx}^{ch} without further information, since both contributions could in principle account for a maximum. However, more can be learned from data on untwined single crystals of YBCO. In particular, the chain contribution k_{xx}^{ch} to the thermal conductivity has been determined from the a-b anisotropy of k_{xx} in a detwined crystal of YBCO [7,11]. Remarkably, k_{xx}^{ch} shows a pronounced maximum below T_{c} with an overall temperature dependence similar to that found here for k_{xx}^{rest} (see Fig. 17). This suggests that the maximum of k_{xx}^{rest} is due to the chain contribution.

Minor differences between k_{xx}^{ch} and k_{xx}^{rest} appear in a more detailed comparison. For example, the maximum of k_{xx}^{rest} is at somewhat higher temperatures than that of k_{xx}^{ch} of reference [11]. Moreover, the relative height of
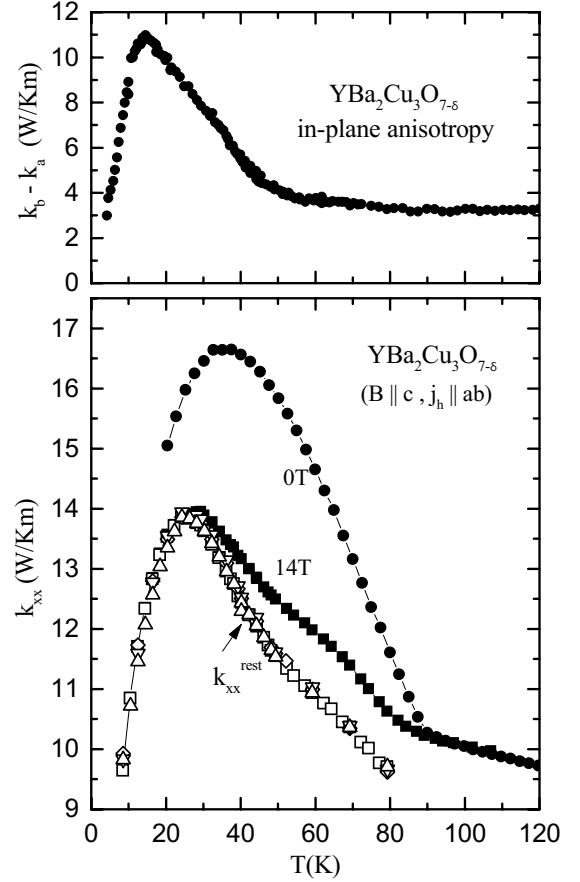

Fig. 17. Upper panel: $k_b - k_a$ as a function of temperature (taken from Ref. [11]). Lower panel: $k_{xx}(B)$ and k_{xx}^{rest} as a function of temperature for YBCO. The different symbols for k_{xx}^{rest} correspond to different magnetic fields. (See text.)

the maximum is smaller. However, firstly k_{xx}^{rest} contains also the phononic contribution, and therefore the relative variations must be smaller than those of k_{xx}^{ch}. Secondly, in a twined crystal defect scattering should be more pronounced. Since the maximum of k_{xx}^{ch} must be attributed to an increase of the QP relaxation time similar to that in the CuO$_2$-planes we suggest that this defect scattering leads to a cutoff for the increase of the QP relaxation time on the chains at lower temperatures, resulting in a smaller height of the maximum and a shift to higher temperatures.

The magnitude of the chain contribution to both, σ_{xx} and k_{xx} is indeed surprising. Naively, one expects that even very weak impurity scattering on the chains suppresses the chain contribution dramatically. Nevertheless, the data on the resistivity and thermal conductivity anisotropy are unambiguous in signaling a sizeable contribution.

Our results have also implications for the phononic contribution to the heat current. Our data suggest that k_{xx}^{ph} is field independent. We note that the latter conclusion has recently been drawn on the basis of low temperature results in Bi-based HTSCs [50]. In principle, k_{xx}^{ph} can be determined experimentally from k_{xx}^{rest}, if one measures k_{xx}^{chain} from the in-plane anisotropy. This requires
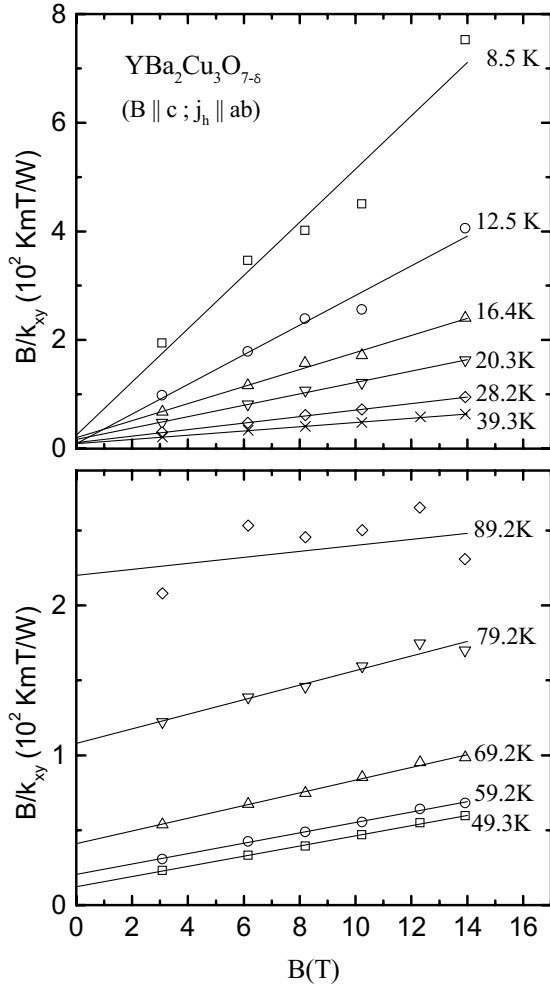
Fig. 18. B/k_{xy} of YBCO as a function of magnetic field for various fixed temperatures given in the figure. Note that the curves extrapolate to (nearly) zero for $T \ll T_c$, which signals a very weak impurity scattering rate (see text).

measurements and an analysis similar as presented here on a detwined crystal.

7.4 Magnetic field dependence of $\underline{k}$

The magnetic field dependence of k_{xy}/B reflects the B-dependence of the electronic heat current below T_c. We recall that k_{xy}/B has the same B-dependence as k_{xx}^{el} (and thus as k_{xx}) (see Eqs. (22, 24) and Fig. 14). For a detailed analysis of the field-dependence of the electronic heat current below T_c it is therefore convenient to analyse k_{xy}/B. We show a representative selection of data in Figures 18 and 19, where we plot B/k_{xy} *versus* B. Obviously, B/k_{xy} varies linearly with B, *i.e.*

$$\frac{B}{k_{xy}} = c_1 + c_2 B, \qquad (33)$$

where c_1 and c_2 depend on temperature, but are field-independent. Our data show that (1) close to T_c and in
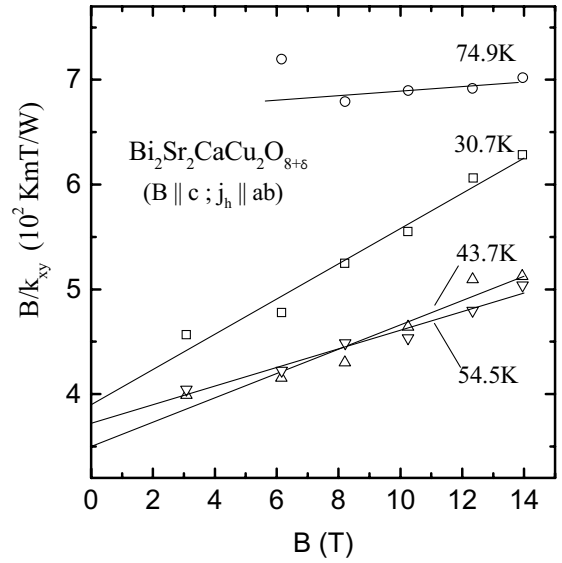

Fig. 19. B/k_{xy} of BSCCO as a function of magnetic field for various fixed temperatures given in the figure. Note the large and nearly temperature independent intersections of the curves, which signal a rather strong impurity scattering rate (see text).

the normal state $B/k_{xy} \simeq c_1$ (*i.e.* $k_{xy} \propto B$ as expected). (2) For $T \ll T_c$, c_1 is very small in YBCO, but it stays large in BSCCO, where the constant and the linear term are of comparable magnitude.

A magnetic field dependence of B/k_{xy} can arise from a field dependence of either the QP-scattering time τ or of the QP-density n_{QP} (or of both). One way to see this is by noting that

$$k_{xy} = k_{xx}^{el}\omega_c\tau_H = LT\sigma_{xx}\omega_c\tau_H = LT\frac{n_{QP}e^2\tau}{m^*}\omega_c\tau_H. \quad (34)$$

This yields

$$\frac{B}{k_{xy}} = C(T)\frac{1}{n_{QP}}\frac{1}{\tau}, \qquad (35)$$

where $C(T) = m^{*2}/LTe^3\tau_H$ depends only on temperature.

We discuss briefly the origin of a magnetic field dependence of n_{QP} and of τ. It seems by now settled that the cuprates are d-wave superconductors, in particular due to an overwhelming body of evidence from experiments sensitive to the phase of the order parameter [62,63]. It has been realized recently that the QP excitation spectrum of an unconventional superconductor with nodes of the order parameter is changed when a magnetic field is applied [64]. The reason is that the circulating supercurrents around the vortices and the corresponding Doppler shift of the QP excitation energies lead to an increase of the number of QPs. In a pure d-wave superconductor the enhancement has been predicted to be proportional to $\sqrt{B}$. Experimentally such an enhancement has been observed in studies of the specific heat at low temperatures [65–68]. At high temperatures an enhancement of n_{QP} by an applied magnetic field should still be present. However, one

expects that in this case the QP-density in a d-wave superconductor is already large in zero magnetic field due to thermal excitation so that the change of n_{QP} due to an applied magnetic field is not so important.

A magnetic field dependence of the scattering time of the QPs below T_c may arise from QP scattering on vortices [10,22,26,61,69–71]. We introduce the QP vortex scattering rate as

$$\tau_v^{-1} = \Sigma_v n_v v_{QP} = \Sigma_v \frac{B}{\Phi_0} v_{QP}. \tag{36}$$

Here v_{QP} is the QP velocity, Σ_v is the scattering cross section of a vortex (per unit length) and $n_v = B/\Phi_0$ is the vortex (areal) density. We assume also that the vortices are disordered so that no Bloch-states form. If the scattering of the QPs is *via* Andreev-scattering on the velocity field associated with the vortices [71] one expects

$$\Sigma_v \propto a_v \propto \sqrt{\frac{\Phi_0}{B}} \tag{37}$$

where a_v is the (average) distance between vortices. This yields $\tau_v^{-1} \propto \sqrt{B}$. On the other hand, one may also imagine scattering of QPs on vortices with a B-independent scattering cross section, *e.g.* due to scattering of QPs on the vortex cores. This leads to $\tau_v^{-1} \propto B$.

We write for the total scattering rate below T_c:

$$\tau^{-1} = \tau_0^{-1} + \tau_i^{-1} + \tau_v^{-1}. \tag{38}$$

Here τ_0^{-1} is an impurity scattering rate independent of B and T and τ_i^{-1} describes the same inelastic scattering processes as in the normal state. τ_i^{-1} collapses below T_c according to our results. Apparently, our experimental results ((Eq. (33)) can be understood if we assume that $\tau_v \propto B$ and that n_{QP} is field independent. We note that it has recently been pointed out by Vekhter and Houghton [70] that indeed at high temperatures the main effect of vortices is to introduce a new scattering time. Our results are not in favor of Andreev-scattering of QPs on vortices, since $\tau_v \propto B$ implies a B-independent scattering cross section.

Accepting that in the temperature range of interest the magnetic field dependence of k_{xy}/B and of k_{xx} can be attributed to a magnetic field dependence of the scattering rate *via* QP-vortex-scattering, while n_{QP} is roughly B-independent, it is possible to explain the differences of the magnetic field dependence between YBCO and BSCCO. Since according to our findings τ_i^{-1} collapses below T_c in both, YBCO and BSCCO, we have $\tau^{-1} \approx \tau_0^{-1} + \tau_v^{-1}(B)$ sufficiently far below T_c. Apparently, the larger value of c_1 in BSCCO (see Eq. (33)) implies that τ_0^{-1} is much more important in BSCCO than in YBCO. This is consistent with the stronger impurity scattering (larger normal state resistivity) in BSCCO. This large impurity scattering rate has several consequences: (1) It serves as a cutoff for the relaxation time below T_c and it decreases the total electronic thermal conductivity, so that phonons are more important in BSCCO. This explains why the maximum of
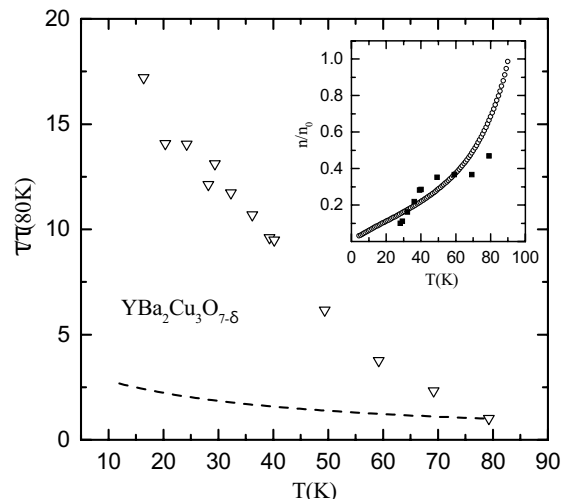

Fig. 20. Quasiparticle scattering time $\tau/\tau(80\ \text{K})$ *versus* temperature for YBCO (triangles). Dashed line: Extrapolation of the normal state behavior of τ obtained from $\sigma_{xx}(T)$. Insert: QP-density n/n_0 as obtained from k_{xx}^{el} and τ (full symbols) and from microwave measurements of the London penetration depth (open symbols) [72]. $n_0 = n(T_c)$ is the normal state charge carrier density.

k_{xx} below T_c is much less pronounced in BSCCO than in YBCO. (2) The scattering on vortices does not dominate the total scattering rate in BSCCO and therefore the magnetic field dependence of k_{xx} and the non-linear behavior of k_{xy} are much weaker in BSCCO than in YBCO. It is only at high magnetic fields where non-linear behavior of k_{xy} occurs in BSCCO, since the vortex scattering becomes more important with increasing B.

The weak impurity scattering in YBCO allows for a rather straightforward estimate of the inelastic scattering time τ_i below T_c. For weak impurity scattering we have $\tau^{-1} \simeq \tau_i^{-1} + \tau_v^{-1} = \tau_i^{-1} + \gamma B$ where γ is a constant. This yields

$$\frac{B}{k_{xy}} = \frac{C(T)}{n_{QP}(T)} \left(\tau_i^{-1} + \gamma B \right) \tag{39}$$

from equation (35). If we assume that γ is independent of temperature, $\tau_i(T)$ can be extracted from the slope and the intersection of the B/k_{xy}-curves (to within the constant factor γ). The result is shown in Figure 20. It confirms that τ_i increases strongly below T_c. Note that no assumption on the temperature dependence of the number of QPs is necessary for this analysis. *Vice versa*, from τ and k_{xx}^{el} the QP-density can be calculated (see Fig. 20).

We finally mention a related topic. It has been pointed out by Simon and Lee [51] that in a magnetic field the QP spectrum and dynamics in a 2 dimensional d-wave superconductor exhibits scaling behavior at low temperatures with respect to $B^{1/2}$. In particular, k_{xy} has been found to scale according to $k_{xy} = T^2 F(\alpha T/B^{1/2})$. Here α is a constant and F is a scaling function. Our low temperature data in YBCO depend on temperature, but not on magnetic field for $B \geq 2-3$ T, which is inconsistent with such

206

a scaling behavior. However, defect scattering is expected to change the possible scaling behavior strongly [69].

7.5 Normal state behavior of $\underline{k}$

7.5.1 Two relaxation times

The necessity to distinguish two relaxation times for the thermal transport effects is consistent with a more detailed analysis of our normal state data. We assume that the carrier densities and the effective masses are comparable in YBCO and BSCCO, since both samples are optimally doped. Using $\sigma_{xx} = ne^2\tau/m$ and $\sigma_{xy}/\sigma_{xx} = \omega_c\tau_H$, the data of Table 1 yield at 100 K:

$$\sigma_{xx}^Y \ \sigma_{xx}^{Bi} \simeq \tau^Y \ \tau^{Bi} \simeq 4 \quad \text{and} \quad \tau_H^Y \ \tau_H^{Bi} \approx 1. \quad (40)$$

For the ratio of the transverse thermal conductivities we find from our experiments

$$k_{xy}^Y \ k_{xy}^{Bi} \approx 4. \quad (41)$$

According to equation (40) this result is consistent with $k_{xy} \propto \tau\tau_H$. In contrast, in standard transport theory $k_{xy} \approx \tau^2$ and thus $k_{xy}^Y/k_{xy}^{Bi} \propto (\tau^Y/\tau^{Bi})^2$ should be of order 16, in disagreement with the experimental results.

A more detailed investigation of the normal state behavior of the thermal effects with respect to the temperature dependence of k_{xy} is in progress. Such an analysis should provide further important information. In particular, $k_{xy} \propto T\tau\tau_H \propto T^{-2}$ if two relaxation times must be used; instead $k_{xy} \propto T\tau^2 \propto T^{-1}$ if only one relaxation time is necessary. We mention that our data are so far compatible with both temperature dependences when analysed over the limited temperature range of our measurements in the normal state.

7.5.2 Electronic thermal conductivity

We discuss here our results for k_{xx}^{el} above T_c. We have not focused on this temperature range since our data analysis requires k_{xx} to be field dependent, which is the case only below T_c. We show in Figure 21 k_{xx}^{el} as calculated from k_{xy} and the Hall angle according to (see Eq. (20))

$$k_{xx}^{el} = k_{xy}\frac{\sigma_{xx}}{\sigma_{xy}} . \quad (42)$$

Note that in order to obtain the plane contribution in YBCO k_{xx}^{el} as given in Figure 21 should be divided by a factor of order 2, since σ_{xx} in equation (20) has an average contribution from the CuO_2-chains, i.e. $\sigma_{xx} = \sigma_{xx}^{pl} + \langle\sigma_{xx}^{ch}\rangle \approx 2\sigma_{xx}^{pl}$, as discussed above. We have, however, not corrected for this factor of 2, since the absolute value of k_{xx}^{el} as calculated from equation (42) is uncertain within a factor of order 2 anyhow due to the uncertainties from the geometric factors in k_{xy}, σ_{xy} and σ_{xx}. Regarding the temperature dependence of k_{xx}^{el} errors in the geometric factor are unimportant. We find that k_{xx}^{el} increases
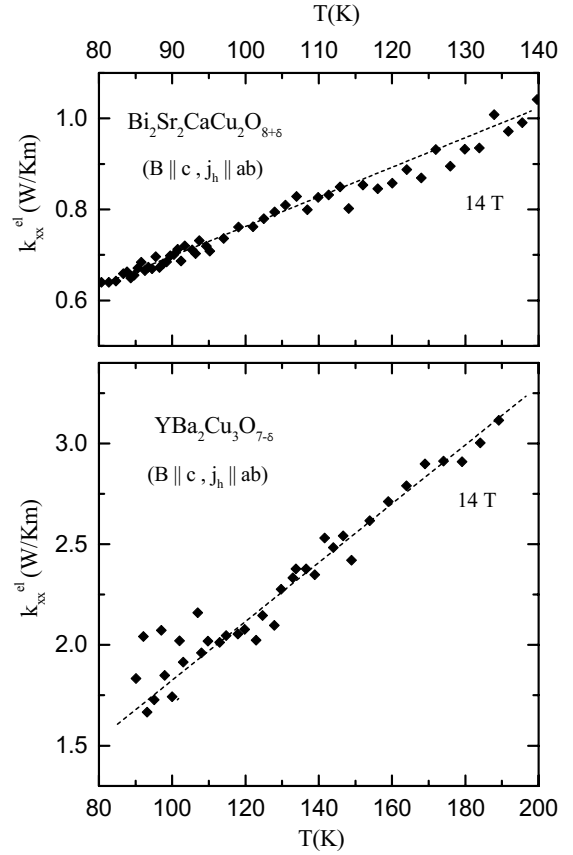

Fig. 21. Electronic thermal conductivity of the CuO_2-planes *versus* temperature as extracted from k_{xy} using the Wiedemann-Franz law. Note the different temperature scale in the upper and lower panel. In order to obtain the plane contribution of k_{xy}^{el} the data for YBCO should be divided by a factor of order 2. (See text.)

(roughly linearly) with temperature. Note that with the transverse Lorenz number $L_{xy} = k_{xy}/T\sigma_{xy}$ we may also write equation (42) as

$$k_{xx}^{el} = L_{xy}T\sigma_{xx}. \quad (43)$$

Since in YBCO $\sigma_{xx} \propto T^{-1}$ and the residual resistivity is small we conclude that L_{xy} increases similarly as k_{xx}^{el} with temperature, roughly as $L_{xy} \propto T$. An increase $L_{xy} \propto T$ in YBCO up to a temperature of 300 K has recently been reported also by Zhang et al. [30].

This increase of k_{xx}^{el} and L_{xy} with temperature is unusual and so far not understood. A temperature dependence of the Lorenz number at intermediate temperatures of order 100–200 K occurs also in conventional metals and is due to the influence of inelastic (usually electron phonon) scattering processes [56]. However, in the cuprates the strong temperature dependence of L_{xy} persists up to 300 K. At these temperatures the Wiedemann Franz law is usually valid in conventional metals. Note that the failure of the Wiedemann Franz law found here implies that a calculation of the temperature dependent

electronic thermal conductivity from the resistivity on the basis of the Wiedemann Franz law with $L_{xx} = L_0$ is not possible.

8 Summary

We have presented a study of the thermal conductivity k_{xx} and of the thermal Hall effect k_{xy} in Y- and Bi-based high temperature superconductors. In both materials k_{xx} and k_{xy} are found to increase below T_c and to show a maximum in their temperature dependence. In addition unusual magnetic field dependence occurs in the superconducting state: The maximum of k_{xx} is strongly suppressed by a magnetic field and k_{xy} varies non-linearly with B.

In the high-T_c superconductors k_{xx} has an electronic and a phononic contribution. The latter dominates in the normal state. In contrast, the transverse thermal conductivity k_{xy} is purely electronic. The strong increase of k_{xy} below T_c therefore gives direct evidence for a strong enhancement of the quasiparticle contribution to the heat current and thus for a strong increase of the quasiparticle mean freepath. From this two important conclusions emerge: Firstly, the main source of quasiparticle scattering in the cuprates is electronic in origin. Secondly, our results confirm that below T_c well defined quasiparticles exist in $Bi_2Sr_2CaCu_2O_{8+\delta}$ and $YBa_2Cu_3O_{7-\delta}$, in agreement with results from photoemission and microwave conductivity.

Using k_{xy} and the magnetic field dependence of k_{xx} we have separated the electronic thermal conductivity (k_{xx}^{el}) of the CuO_2-planes from the phononic thermal conductivity (k_{xx}^{ph}). In $YBa_2Cu_3O_{7-\delta}$ k_{xx}^{el} shows a pronounced maximum in the superconducting state. This maximum is much weaker in $Bi_2Sr_2CaCu_2O_{8+\delta}$, which we attribute to stronger impurity scattering in $Bi_2Sr_2CaCu_2O_{8+\delta}$. An additional magnetic field independent contribution to the maximum of k_{xx} occurs in $YBa_2Cu_3O_{7-\delta}$, reminiscent of the contribution of the CuO-chains, as determined from the anisotropy in untwined single crystals. Our data analysis reveals that below T_c as in the normal state a transport (τ) and a Hall (τ_{H}) relaxation time must be distinguished: The inelastic (*i.e.* temperature dependent) contribution to τ is strongly enhanced in the superconducting state, whereas τ_{H} displays the same temperature dependence above and below T_c.

The unusual magnetic field dependence of k_{xx} and k_{xy} below T_c can be attributed to a B-dependent QP scattering time. We suggest that the origin is the scattering of quasiparticles on vortices. Our data give evidence that the corresponding QP-vortex scattering rate varies linearly with B.

Finally, we have calculated the electronic thermal conductivity from the transverse effects also in the normal state. We find that k_{xx}^{el} and the (transverse) Lorenz number increase roughly linearly with temperature. This implies in particular that the Wiedemann-Franz law is not valid in the normal state.

References

1. For a review of early work see *e.g.* C. Uher, in *Physical Properties of High Temperature Superconductors*, edited by D.M. Ginsberg (World Scientific, Singapore, 1992), Vol. 3.
2. S.J. Hagen, Z.Z. Wang, N.P. Ong, Phys. Rev. B **40**, 9389 (1989).
3. T.T.M. Palstra, B. Batlogg, L.F. Schneemeyer, J.V. Waszczak, Phys. Rev. Lett. **64**, 3090 (1990).
4. R.A. Richardson, S.D. Peacor, F. Nori, C. Uher, Phys. Rev. Lett. **67**, 3856 (1991).
5. S.D. Peacor, J.L. Cohn, C. Uher, Phys. Rev. B **43**, 8721 (1991).
6. S.D. Peacor *et al.*, Phys. Rev. B **44**, 9508 (1991).
7. R.C. Yu, M.B. Salamon, J.P. Lu, W.C. Lee, Phys. Rev. Lett. **69**, 1431 (1992).
8. J.L. Cohn, E.F. Skelton, S.A. Wolf, J.Z. Liu, R.N. Shelton, Phys. Rev. B **45**, 13144 (1992).
9. J.L. Cohn, S.A. Wolf, T.A. Vanderah, V. Selvamanickam, K. Salama, Physica C **192**, 435 (1992).
10. M.B. Salamon, F. Yu, V.N. Kopylov, J. Superconduct. **8**, 449 (1995).
11. R. Gagnon, S. Pu, B. Ellman, L. Taillefer, Phys. Rev. Lett. **78**, 1976 (1997).
12. K. Takenaka, Y. Fukuzumi, K. Mizuhashi, S. Uchia, H. Asaoka, H. Takei, Phys. Rev. B **56**, 5654 (1997).
13. H. Aubin, K. Behnia, M. Ribault, R. Gagnon, L. Taillefer, Phys. Rev. Lett. **78**, 2624 (1997).
14. A.N. Taldenkov, P. Esquinazi, K. Leicht, J. Low Temp. Phys. **115**, 15 (1999).
15. D.A. Bonn, W.N. Hardy, in *Physical Properties of High Temperature Superconductors*, edited by D.M. Ginsberg (World Scientific, Singapore, 1996), Vol. 5
16. M.C. Nuss, P.M. Mankiewich, M.L. O'Malley, E.H. Westerwick, P.B. Littlewood, Phys. Rev. Lett. **66**, 3305 (1991).
17. D.B. Romero, C.D. Proter, D.B. Tanner, L. Forro, D. Mandrus, L. Mihaly, G.L. Carr, G.P. Williams, Phys. Rev. Lett. **68**, 1590 (1992).
18. D.A. Bonn, P. Dosanjh, R. Liang, W.N. Hardy, Phys. Rev. Lett. **68**, 2390 (1992).
19. D.A. Bonn, R. Liang., T.M. Riseman, D.J. Baar, D.C. Morgan, K. Zhang, P. Dosanjh, T.L. Duty, A. MacFarlane, G.D. Morris, J.H. Brewer, W.N. Hardy, Phys. Rev. B. **47**, 11314 (1992).
20. M.J. Graf, S.-K. Yip, J.A. Sauls, D. Rainer, Phys. Rev. B **53**, 15147 (1996).
21. B. Serin, in *Superconductivity*, edited by R.D. Parks (Dekker, New-York, 1969), p. 925.
22. W.F. Vinen, E.M. Forgan, C.E. Gough, M.J. Hood, Physica **55**, 94 (1971).
23. O. Baberski, A. Lang, O. Maldonado, M. Hücker, B. Büchner, A. Freimuth, Europhys. Lett. **44**, 335 (1998).

208

24. J.L. Cohn, C.K. Lowe-Ma, T.A. Vanderah, Phys. Rev. B **52**, R13134 (1995).
25. A. Freimuth, M. Galffy, C. Hohn, B. Zeini, J. Low Temp. Phys. **95**, 383 (1994).
26. K. Krishana, J.M. Harris, N.P. Ong, Phys. Rev. Lett. **75**, 3529 (1995).
27. B. Zeini, A. Freimuth, B. Büchner, R. Gross, A.P. Kampf, M. Kläser, G. Müller-Vogt, Phys. Rev. Lett. **82**, 2175 (1999).
28. B. Zeini, A. Freimuth, B. Büchner, R. Gross, A.P. Kampf, M. Kläser, G. Müller-Vogt, Physica C **317-318**, 325 (1999). Note that there is a mistake in Figures 3 and 4 of this paper: The factor of 10^{-2} in the labeling of k_{xy} in Figure 3 and of k_{xy}/B in Figure 4 should be ommitted.
29. K. Krishana, N.P. Ong, Y. Zhang, Z.A. Xu, R. Gagnon, L. Taillefer, Phys. Rev. Lett. **82**, 5108 (1999).
30. Y. Zhang, N.P. Ong, Z.A. Xu, K. Krishana, R. Gagnon, L. Taillefer, Phys. Rev. Lett. **84**, 2219 (2000).
31. U. Welß, S. Fleshler, W.K. Kwok, J. Downey, Y. Fang, G.W. Crabtree, J.Z. Liu, Phys. Rev. B **42**, 10189 (1990).
32. T.A. Friedmann, M.W. Rabin, J. Giapintzakis, J.P. Rice, D.M. Ginsberg, Phys. Rev. B **42**, 6217 (1990).
33. Y. Iye, in *Physical Properties of the High Temperature Superconductors*, edited by D.M. Ginsberg (World Scientific, Singapore, 1992), Vol. 3, p. 285.
34. T.R. Chien, Z.Z. Wang, N.P. Ong, Phys. Rev. Lett. **67**, 2088 (1991).
35. A. Freimuth, in *Superconductivity, Frontiers in Solid State Sciences*, edited by L.C. Gupta, M.S. Multani (World-Scientific, Singapore, 1992), p. 393.
36. A. Freimuth, M. Zittartz, Phys. Rev. Lett. **84**, 4978 (2000).
37. A. Freimuth, B. Zeini, submitted to Phys. Rev. B.
38. See *e.g.* A.A. Abrikosov, *Fundamentals of the Theory of Metals* (Elsevier Science Publishing Co., New York, 1988).
39. It is also possible to attribute the temperature dependence of R_H to a temperature dependent effective mass; see *e.g.* D.B. Romero, Phys. Rev. B **46**, 8505 (1992).
40. P.W. Anderson, Phys. Rev. Lett. **67**, 2092 (1991).
41. P. Coleman, A.J. Schofield, A.M. Tsvelik, Phys. Rev. Lett. **76**, 1324 (1996).
42. P. Coleman, A.J. Schofield, A.M. Tsvelik, J. Phys. Cond. Matt. **8**, 9985 (1996).
43. A. Carrington, A.P. Mackenzie, C.T. Lin, J.R. Cooper, Phys. Rev. Lett. **69**, 2855 (1992).
44. R. Hlubina, T.M. Rice, Phys. Rev. B **51**, 9253 (1995).
45. B.P. Stojković, D. Pines, Phys. Rev. Lett. **76**, 811 (1996); Phys. Rev. B **55**, 8576 (1997).
46. See also the comment by N.P. Ong, P.W. Anderson, Phys. Rev. Lett. **78**, 977 (1997) and the reply by B. P. Stojković, D. Pines, *ibid.* **78**, 978 (1997).
47. L.B. Ioffe, A.J. Millis, Phys. Rev. B **58**, 11631 (1998).
48. A.T. Zheleznyak, V.M. Yakovenko, H.D. Drew, I.I. Mazin, Phys. Rev. B **57**, 3089 (1998).
49. A.T. Zheleznyak, V.M. Yakovenko, H.D. Drew, Phys. Rev. B **59**, 207 (1999).
50. K. Krishana, N.P. Ong, Q. Li, G.D. Gu, N. Koshizuka, Science **277**, 83 (1997).
51. S.H. Simon, P.A. Lee, Phys. Rev. Lett. **78**, 1548 (1997).
52. M. Zeh, H.-C. Ri, F. Kober, R.P. Huebener, A.V. Ustinov, J. Mannhart, R. Gross, A. Gupta, Phys. Rev. Lett. **64**, 3195 (1990).
53. M. Galffy, A. Freimuth, U. Murek, Phys. Rev. B **41**, 11029 (1990).
54. C. Hohn, M. Galffy, A. Dascoulidou, A. Freimuth, H. Soltner, U. Poppe, Z. Phys. B **85**, 161 (1991).
55. H.C. Ri, R. Gross, F. Gollnik, A. Beck, R.P. Huebener, P. Wagner, H. Adrian, Phys. Rev. B **50**, 3312 (1994).
56. For a detailed discussion see *e.g.* J. Ziman, *Electrons and Phonons* (Oxford University, New York, 1960).
57. M. Randeria, H. Ding, J.-C. Campuzano, A. Bellman, G. Jennings, T. Yokoya, T. Takahashi, H. Katayama-Yoshida, T. Mochiku, K. Kadowaki, Phys. Rev. Lett. **74**, 4951 (1995).
58. A. Kaminski, J. Mesot, H. Fretwell, J.C. Campuzano, M.R. Norman, M. Randeria, H. Ding, T. Sato, T. Takahashi, T. Mochiku, K. Kadowaki, H. Hoechst, Phys. Rev. Lett. **84**, 1788 (2000).
59. P.J. Hirschfeld, W.O. Putikka, Phys. Rev. Lett. **77**, 3909 (1996).
60. J.M. Harris, N.P. Ong, P. Matl, R. Gagnon, L. Taillefer, T. Kimura, K. Kitazawa, Phys. Rev. B **51**, 12053 (1995).
61. R.M. Cleary, Phys. Rev. **175**, 587 (1968).
62. See *e.g.* D.J. van Harlingen, Rev. Mod. Phys. **67**, 515 (1995).
63. D.J. Scalapino, Phys. Rep. **250**, 329 (1995).
64. G.E. Volovik, JETP Lett. **58**, 469 (1993).
65. K.A. Moler, D.J. Baar, J.S. Urbach, R.Liang, W.N. Hardy, A. Kapitulnik, Phys. Rev. Lett. **73**, 2744 (1994).
66. K.A. Moler, D.L. Sisson, J.S. Urbach, M.R. Beasley, A. Kapitulnik, D.J. Baar, R. Liang, W.N. Hardy, Phys. Rev. B **55**, 3954 (1997).
67. B. Revaz, J.-Y. Genoud, A. Junod, K. Neumaier, A. Erb, E. Walker, Phys. Rev. Lett. **80**, 3364 (1998).
68. D.A. Wright, J.P. Emerson, B.F. Woodfield, J.E. Gordon, R.A. Fisher, N.E. Philips, Phys. Rev. Lett. **82**, 1550 (1999).
69. C. Kübert, P.J. Hirschfeld, Phys. Rev. Lett. **80**, 4963 (1998).
70. I. Vekhter, A. Houghton, Phys. Rev. Lett. **83**, 4626 (1999).
71. M. Franz, Phys. Rev. Lett. **82**, 1760 (1999).
72. W.N. Hardy, D.A. Bonn, D.C. Morgan, R. Liang, K. Zhang, Phys. Rev. Lett. **70**, 3999 (1993).